TAMPEREEN TEKNILLINEN YLIOPISTO
TAMPERE UNIVERSITY OF TECHNOLOGY
Julkaisu 627 • Publication 627

Veer D. S. Dhaka

Ultrafast Capture and Relaxation of Carriers in InGaAs Semiconductor Quantum Well Nanostructures

Tampere 2006

Tampereen teknillinen yliopisto. Julkaisu 627
Tampere University of Technology. Publication 627

Veer D. S. Dhaka

Ultrafast Capture and Relaxation of Carriers in InGaAs Semiconductor Quantum Well Nanostructures

Thesis for the degree of Doctor of Technology to be presented with due permission for public examination and criticism in Festia Building, Auditorium Pieni Sali 2, at Tampere University of Technology, on the 3rd of November 2006, at 12 noon.

Tampereen teknillinen yliopisto - Tampere University of Technology
Tampere 2006

ISBN 952-15-1668-2 (printed)
ISBN 952-15-1748-4 (PDF)
ISSN 1459-2045

Abstract

Development of high-speed electronic and optoelectronic devices based on semiconductor quantum wells requires clear understanding of the dynamics and kinetics of carrier transport and relaxation on an ultra short time scale. The carrier capture and the decay times are the two most important parameters that decide the dynamic performance of the devices. This Thesis is devoted to study the carrier dynamics in various MBE grown compound semiconductors, such as InGaAs/GaAs, InGaAs/InP and InGa(N)As/GaAs QW structures. The temporal evolution of non-equilibirium carriers in QWs samples was monitored using a femtosecond up-conversion technique.

The as-grown QW structures show decay time values ranging from 500 to1000 ps, which is far too long for ultrafast operations. The aim of this study was to make the semiconductors faster by reducing this decay time values to sub-picosecond levels using the ion implantation technique and to investigate systematically the influence of intentionally created defects and post-irradiated annealing on carrier capture and relaxation process in a wide range of QW samples. The effect of different ion species, implantation energy, dose and annealing on decay and capture processes are studied in detail. The main findings are that sub-picosecond lifetimes of choice could be achieved in InGaAs/GaAs and InGaAs/InP structures at appropriate dose, implantation energy, and annealing conditions. We have observed that heavy ion created defects are not thermally stable with time for a certain period after the irradiation and show room temperature ageing. Among the different light and heavy ions used for implantation, irradiation with Ne^+ ion was found to be considerably more effective than the others, which is a good alternative to the more traditional Ni^+-irradiation.

The QWs collect only those carriers, which are created near the QW interfaces. The capture as well the decay time was found to decrease with the dose. Annealing was found to increase the lifetimes appreciably in all the irradiated structures but the capture profile of carriers in the QW was found to be independent of annealing in almost all of the structures studied. This suggests that ion implantation creates shallow traps near the barrier and QW region and deep centers far from the barriers. Mainly the shallow traps affect the capture dynamics, while mainly the deep traps affect the decay of carriers. The QW samples prepared and studied in this Thesis were aimed for the active region of SESAMs devices. Furthermore, the comprehensive details and mechanism for carrier transport and relaxation in QW heterostructures is investigated in depth. Precise values of decay and capture time for InGaAs/GaAs, InGaAs/InP, and InGa(N)As/GaAs samples are reported with irradiation dose, light and heavy ion species, implantation energy, MBE growth temperature and annealing as the main parameters.

Preface

This research work has been carried out at the Institute of Materials Chemistry (IMC), in collaboration with Optoelectronics Research centre (ORC) of Tampere University of Technology, Finland between October 2003 and October 2006.

I wish to express my deepest gratitude to my supervisor Prof. Helge Lemmetyinen, Head of the Institute (IMC), for giving me the opportunity to work in the field of semiconductor's *via* TULE/QUEST project, for supporting me financially through different sources. He gave me absolute free hand on small and big matters, during my entire stay at IMC. Often I have felt privileged to be him as my supervisor. I am especially grateful to my co-supervisor Dr. Nikolai V. Tkachenko for all the practical and technical help. His outstanding expertise and knowledge on science and beyond was a source of inspiration. He always, anywhere and anytime, has time to discuss scientific things with me. His cool patience and ready to help nature in any kind of situation is one of the things I will never forget.

I am grateful to Prof. Markus Pessa, Director and Head of ORC, for spending his considerable time in polishing and re-writing almost all my manuscripts. It would not have been possible to publish these papers in a short period of time without his help and knowledge. My special thanks goes to our collaborators Dr. Kai Arstila, Prof. Kai Nordlund and Prof. Juhani Keinonen of Accelarator Laboratory, University of Helsinki for their help and fruitful discussion on ion irradiation related issues.

I am grateful to Mr. Atul Khanna, Director Tooltech Software (India), for sending me to Finland. This Thesis simply wouldn't happen without him. I am thankful to Mr. Anil Talwani, Country Manager Tooltech, for his help and discussion on various matters other than science.

I would like to thank all of my colleagues and members at IMC for providing a pleasant research environment. In particular, I would like to mention Dr. Tommi Vuorinen for his friendly help during my entire stay at IMC. I am thankful to Vladimir Chukharev, Oana Cramariuc, Temmu Toivonen, Kalle Lintinen, Kimmo Kaunisto for their help and tips on Finland. My work has benefited a lot from the fruitful research cooperation with Dr. Emil-Mihai Pavelescu (ORC) and Dr. Mircea Guina (ORC).

Above all, my warmest thanks goes to my parents. I have always felt their endless love accompanying me and supporting me. I would especially like to mention my little village in India, "Dhikauli", where I grew up and have fond childhood memories. I am indebted for the endless love and encouragement from my Wife, Deepti, for caring and understanding me. Also, warmest thanks to my younger brother, back home.

October 2006

Tampere, Finland

V.D.S. Dhaka

List of publications

This Thesis consists of the following papers:

[P1] **V. D. S. Dhaka**, N. V. Tkachenko, E. -M. Pavelescu, H. Lemmetyinen, T. Hakkarainen, M. Guina, J. Konttinen, O. Okhotnikov, M. Pessa, K. Arstila and J. Keinonen, "*Ni^+-irradiated InGaAs/GaAs quantum-wells: picosecond carrier dynamics*", **New J. Phys.**, vol. 7, 131, 2005.

[P2] **V. D. S. Dhaka**, N.V. Tkachenko, H. Lemmetyinen, E. -M. Pavelescu, J. Konttinen, M. Pessa, K. Arstila and J. Keinonen, "*Room-temperature self-annealing of heavy-ion-irradiated InGaAs/GaAs quantum wells* **"**, **IEE Electron. Lett.**, vol. 41, pp. 1304-1305, 2005.

[P3] T. Hakkarainen, E. -M. Pavelescu, K. Arstila, **V. D. S. Dhaka**, T. Hakulinen, R. Herda, J. Konttinen, N. Tkachenko, H. Lemmetyinen, J. Keinonen and M. Pessa, "*Optical properties of ion irradiated and annealed InGaAs/GaAs quantum wells and semiconductor saturable absorber mirrors***", J. Phys. D: Appl. Phys.**, vol. 38, pp. 985-989, 2005.

[P4] E. -M. Pavelescu, T. Hakkarainen**, V. D. S. Dhaka**, N. V. Tkachenko H. Lemmetyinen, T. Jouhti and M. Pessa**,** "*Influence of As pressure on photoluminescence and structural properties of GaInNAs/GaAs quantum wells grown by molecular beam epitaxy"*, **J. Crystal Growth**, vol. 281, pp. 249-254, 2005.

[P5] **V. D. S Dhaka**, N. V. Tkachenko, H. Lemmetyinen, E. -M. Pavelescu, S. Suomalainen, M Pessa, K. Arstila, K. Nordlund and J. Keinonen, "*Ultrafast dynamics of Ni^+-irradiated and annealed GaInAs/InP multiple quantum wells"*, **J. Phys. D: Appl. Phys.**, vol. 39, pp. 2659-263, 2006.

[P6] **V. D. S. Dhaka**, N. V. Tkachenko, H. Lemmetyinen, E. -M. Pavelescu, M. Guina, A. Tukiainen J. Konttinen, M. Pessa, K. Arstila, J. Keinonen and K. Nordlund, "*Effects of heavy-ion and light-ion irradiation on the room-temperature carrier dynamics of InGaAs/GaAs quantum wells"*, **Semiconductor Science and Technology**, vol. 21, pp. 661-664, 2006.

[P7] **V. D. S. Dhaka**, N. V. Tkachenko, E. -M. Pavelescu, H Lemmetyinen, M. Pessa, "*Effect of growth temperature and post-annealing on carrier dynamics in GaIn(N)As/GaAs quantum wells"*, **Solid State Electronics** (Submitted).

Supplementary publications related to this work but not included in the Thesis:

[SP1] E. -M. Pavelescu, A. Gheorghiu, M. Dumitrescu, A. Tukiainen, T. Jouhti, T. Hakkarainen, R. Kudrawiec, J. Andrzejewski, J. Misiewicz, N. Tkachenko, **V. D. S. Dhaka**, H. Lemmetyinen and M. Pessa, "*Electron-irradiation enhanced photoluminescence from GaInAs/GaAs quantum wells subject to thermal annealing*", **Appl. Phys. Lett**., vol. 85, pp. 6158-6160, 2004.

[SP2] H.F. Liu, C.S. Peng, J. Likonen, J. Konttinen, **V.D.S. Dhaka**, N. Tkachenko and M. Pessa "*Thermal annealing effect on 1.3-mm GaInNAs/GaAs quantum well structures capped with dielectric films*", **IEE Proc. Optoelectron**, vol. 151, pp. 267-270, 2004.

[SP3] C. Bjöörkas, K. Nordlund, K. Arstila, J. Keinonen, **V.D.S. Dhaka** and M. Pessa, "*Damage production in GaAs and GaAsN induced by light and heavy ions*", **J. Appl. Phys.**, vol. 100, pp. 053516, 2006.

[SP4] E.- M. Pavelescu, J. Slotte, **V. D. S. Dhaka**, K. Saarinen, S. Antohe, Gh. Cimpoca and M. Pessa, "*On the optical crystal properties of quantum-well GaIn(N)As/GaAs semiconductors grown by MBE"*, **J. Crystal Growth** , 2006 (Accepted for publication).

Contents

List of Abbreviations

MBE	Molecular beam epitaxy
QW	Quantum well
MQW	Multiple quantum wells
PL	Photoluminescence
TRPL	Time-resolved photoluminescence
RTA	Rapid thermal annealing
RT	Room temperature
SESAM	Semiconductor saturable absorber mirror
VCSEL	Vertical cavity surface emitting lasers
HEMT	High electron mobility transistor
BJT	Bipolar junction transistor
MOSFET	Metal-oxide-semiconductor field-effect transistor
UHV	Ultra-high vacuum
RHEED	Reflection high-energy electron diffraction
AES	Auger electron spectroscopy
XPS	Photoelectron spectroscopy
SIMS	Secondary ion mass spectroscopy

Author's contribution

This research work is carried out within the framework of national TULE/Ultra-fast quantum-regime semiconductors, components, and sub-systems (QUEST) project of the Academy of Finland, in close-knit collaboration with Optoelectronics Research Centre (ORC), Institute of Materials Chemistry (IMC) of the Tampere University of Technology (TUT), and Accelerator Laboratory of the Helsinki University of Technology (HUT).

The work presented here is a result of the efforts of a whole team. Preparation of multiple quantum well samples (including SESAMs devices) by molecular beam epitaxy, and annealing were done at ORC under the leadership of Prof. Markus Pessa. Dr. Kai Arstila, Prof. K. Nordlund and Prof. J. Keinonen of Accelarator Laboratory were responsible for ion irradiation of the samples with different ions. Ultrafast time resolved measurements using the up-conversion and pump-probe techniques were performed at IMC.

V. D. S. Dhaka was responsible for writing the papers 1, 2, 5, 6 & 7 and is the corresponding author. He planned and performed all the time-resolved experiments at IMC in close collaboration with Dr. Nikolai. V. Tkachenko and Prof. Helge Lemmetyinen. He is responsible for analysis and interpretation of all the data. For papers 3 & 4, the author is responsible for the up-conversion measurements and interpretation of the time- resolved data.

1. Introduction

Semiconductors are the foundation of today's information age. Much of the information technology is based on the fast response of small and high speed microelectronic and opto-electronics devices. This ever-demanding need for faster response and faster processing of information is one of the major challenges in the development of semiconductor microelectronics and opto-electronics. For many years there has been considerable interest in exploring the limitations of semiconductors used in this technology by investigating at a fundamental level and the underlying fast microscopic processes, which occur on a picoseconds or even a femtosecond time scale [1-3]. Today however, semiconductor technology has reached a level where the characteristic time scales of the underlying physical processes determine the speed limits. The research and development of such high-speed devices require a clear understanding of the various dynamical properties of carriers in semiconductors on an ultrafast time scale [1-3]. Among various devices exploiting the properties arising from the quantum confinement of the carriers, semiconductor quantum wells are particularly important due to their unique properties and wide applications as active region in optical and electronic devices [4,5].

A quantum well is formed when a narrow bandgap material is sandwiched between the two higher bandgap materials called barriers, where the carriers in the well are restricted to move only in two dimensions giving rise to quantized energy states. The optical excitation of semiconductor structure above the barrier band gap creates non-equilibrium carriers. These hot carriers relax to the lattice temperature and reach the QW *via* different scattering mechanisms involving the transport and relaxation of carriers. The most important parameters that are crucial for the quantum well based devices are the characteristic time limits of these two processes: (1) carrier transport from the barriers followed by their capture into the quantum well, and (2) subsequent decay of these carriers in the well with time. The decay time (lifetime) of carriers determines the fast response of the devices such as saturable absorbers and could be precisely controlled by creation of intentional defects in the semiconductor structure *via* the ion-implantation, while the upper frequency modulation limit in devices such as semiconductor lasers is controlled by the capture time. The time evolutions of capture and decay process is governed by different scattering process in barrier as well as within the well. Typical time scales for the scattering process in semiconductors are in the range of picoseconds or femtoseconds and the resulting dynamics are generally termed *ultrafast.*

Ultrafast laser physics and technology now allow us to study the very initial interaction processes of non-equilibirium carriers in semiconductors. The typical time scales for the fastest processes in semiconductor ranges from a few femtoseconds to picoseconds. With the development of lasers that can generate pulses as short as few femtoseconds, a great deal of insight details of carrier dynamics in semiconductor could be investigated. In other words, the application of time-resolved optical spectroscopy to the study of relaxation and transport dynamics of carriers in semiconductors is closely related to the ability to produce laser pulses on these time scales. One of the first challenges that researchers faced in the early days of the investigation of the photo-excitation of semiconductors by laser pulse was to achieve high temporal resolution. The shorter the duration of the pulse used in the excitation of the material the better the temporal resolution of the various dynamical processes. The motivation was to generate very short optical pulses that would allow researchers to probe faster processes. By the early 1980s this challenge was met with the availability of sub-picosecond laser pulses allowing researchers to use time resolved ultrafast techniques. However, a time-resolved measurement with ultrashort resolution is a formidable task. The traditional approach, which uses high-speed electronic instruments, failed since the response time of such instrumentation is several orders of magnitude slower than the dynamic processes occurring in semiconductors. Novel and precise optical techniques are now being used to explore the properties of semiconductors on a time scale much shorter than those previously believed to be attainable. The developments of excite-and-probe techniques, such as up-conversion and pump-probe, have shown how to probe extremely short-lived processes with resolution limited only by laser pulse itself.

This Thesis deals with the detailed investigation of ultrafast carrier capture and decay dynamics in InGaAs based semiconductor quantum well structures using the femtosecond up-conversion and pump-probe techniques. The samples were grown by molecular beam epitaxy method and mainly consist of InGaAs/GaAs, InGaAs/InP and InGa(N)As/GaAs quantum wells. The goal of this thesis was to study the capture and decay processes of non-equilibrium carriers in different QWs as a function of ion irradiation dose, light and heavy ion species, implantation energy, annealing and MBE growth temperature. The basic mechanism of carrier transport and relaxation in these heterostructures is investigated systematically with precise values of the capture and decay times reported, which could be exploited for designing various opto-electronic and electrical devices, especially saturable absorbers which are based on short recovery times of carriers

in the active region and semiconductor saturable absorber mirrors (SESAMs), which are used as cavity end reflectors for pulse mode locking in solid state and fibre lasers.

2. Background

In this chapter the main theoretical concepts and the techniques used in this Thesis are reviewed. The subjects to be considered are related to:

i) III-V compound semiconductors
ii) Growth by molecular beam epitaxy (MBE)
iii) Quantum confinement effects in semiconductor heterostructures
iv) Creation of defects in quantum well samples: Ion implantation
v) Mode locking and semiconductor saturable absorber mirrors (SESAMs)
vi) Femtosecond photoluminescence (PL) up-conversion technique
vii) Pump-probe technique
viii) Carrier dynamics of QWs

2.1 III-V compound semiconductors

The III-V semiconductor materials are potential candidates for opto-electronic devices, because of their direct bandgap structure [5,6]. These compounds are basically semiconductors that consist of permutations of the column III elements Al, Ga and In, and the column V elements N, P, As and Sb. III-V semiconductors are characterised by their excellent optoelectronic (efficient light emission and absorption) and electronic (high carrier motilities) properties [5, 6]. III-V compound semiconductor materials generally have a zinc blend structure, which is made up out of two face centered cubic units cells, displaced over a quarter diagonal. The optoelectronic applications of the various families of III-V materials are determined in large part by the wavelength ranges within which they emit and absorb light efficiently. GaAs-related materials have a spectral window between 0.8-1 µm and InP-related materials between 1.3-1.7 µm. The thermodynamic stability of most ternary and quaternary alloys provides a wide opportunity for bandgap tuning towards the optical communication wavelength window.

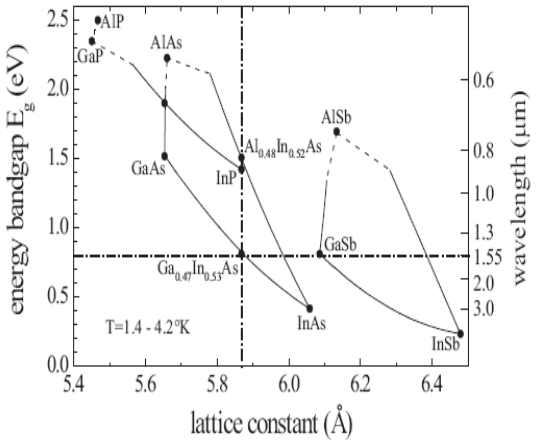

Figure 2.1 Bandgap energy *vs.* lattice constant for various III-V compound semiconductors [4].

The variation of bandgap with respect to the lattice constant for different alloy composition can be read from Figure 2.1. The lattice constants and the band gap energy of the ternary (three components) compounds can be obtained from the binary constituents by Vegard's law [7]. For $In_xGa_{1-x}As$, the lattice constant *a(x)* can be expressed as

$$a(x) = xa^{GaAs} + (1-x)a^{InAs} \tag{2.1}$$

where a^{GaAs}, a^{InAs} are the lattice constant of the binary GaAs and InAs compounds, respectively.

If the energy gaps of GaAs and InAs are denoted as E_g^{GaAs}, E_g^{InAs}, then the bang gap energy (E_g) of the ternary $In_xGa_{1-x}As$ compounds is given by:

$$E_g(x) = xE_g^{GaAs} + (1-x)E_g^{InAs} - cx(1-x) \tag{2.2}$$

where *c* is the bowing parameter. The lattices constants and the band gaps of the other compounds follow from the similar relations.

2.2 Growth by molecular beam epitaxy (MBE)

The molecular beam epitaxy (MBE) is a highly precise and versatile epitaxial crystal growth technique invented by A. Y. Cho at Bell Laboratories [8]. It is an ultrahigh vacuum (UHV) deposition technique and has the ability to prepare epitaxial layers with atomic dimensional precision down to a few angstroms [8]. MBE technology is used in the development of a host of highly efficient optical and electronic devices, such as strained QW lasers, VCSEL's, QW infrared photodetectors, quantum cascade lasers, HEMT, BJT, and MOSFET [9].

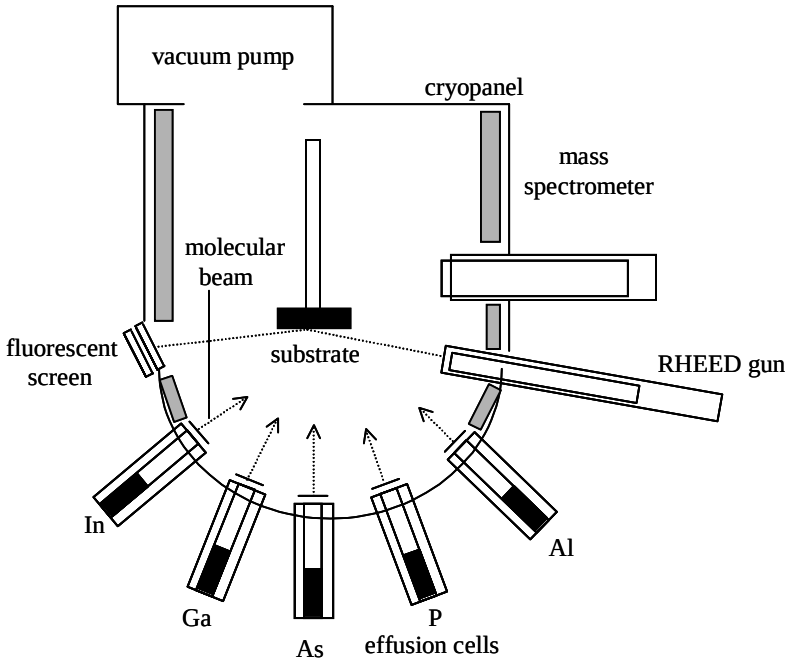

Figure 2.2 Schematic for a simple MBE system.

The main elements of solid source molecular beam epitaxy (SS-MBE) growth chamber are shown in Figure 2.2. Molecular beams, generated by effusion cells, impinge on a crystalline substrate mounted on a rotating holder under ultra-high vacuum (UHV) conditions. The substrate is held at a suitable temperature in order to activate the thermal migration of adsorbed species on the surface. The UHV environment is required in order to reduce the background pressure of contaminants that, otherwise, would be incorporated into the solid phase. To ensure UHV conditions during growth, the chamber is provided with liquid-nitrogen shrouds. Group III and V molecular beams are produced by evaporating or sublimating source materials contained in high purity crucibles in the effusion cells. The fluxes of molecular beams that depend on the temperature of the respective cells are measured by means of an ion-gauge that can be placed in the substrate position. The molecular beams can be interrupted by means of mechanical shutters with actuation times corresponding to those required to deposit less than an atomic layer of material. The UHV environment allows the use of in-situ analysis tools such as Quadruple Mass Analyzers (QMA) to monitor the vacuum environment and Reflection High Energy Electron Diffraction (RHEED) equipments to study the growing surface. Other characterization techniques, such as Auger Electron Spectroscopy (AES), X-ray Photoelectron Spectroscopy (XPS) and Secondary Ion Mass

Spectroscopy (SIMS) are available in the growth chamber or, more frequently, in separate chambers connected to the growth one by UHV modules.

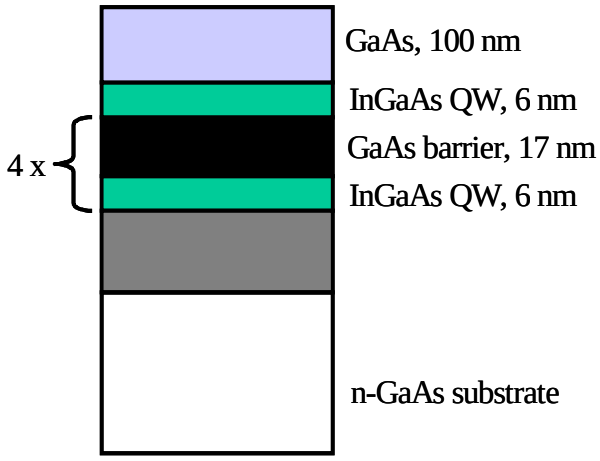

Figure 2.3 InGaAs/GaAs MQW structure grown by MBE.

A typical InGaAs/GaAs QW structure used in this Thesis and grown by MBE is shown in Figure 2.3. The III-V compounds grown by MBE were mainly InGaAs/GaAs, InGaAs/InP and InGa(N)As/GaAs QWs structures.

2.3 Quantum confinement effects in semiconductor heterostructures

The electronic and optical properties of low-dimensional semiconductor structures and semiconductor nanostructures are completely determined by size quantization and confinement effects.

When the thickness L_z of a semiconductor layer is reduced to the order of a carrier de Broglie wavelength ($\lambda = h/p \sim L_z$), effects not typical of the bulk material, known as quantum size effects occur [10-12]. By sandwiching a thin layer of a narrow band gap material between two (normally thicker) layers of a wide gap material, a potential well may be formed (Figure 2.4a). The effect of this potential is to reduce the number of degree of freedom of free carriers in the well, which lies in the narrow gap material. A well is being regarded as narrow if its width is less than the electron de Broglie wavelength. In such cases, the permissible electron energies are quantized along the growth direction, due to the potential energy barriers formed by the wide gap material. The energy levels in a quantum well are determined by its thickness and its depth. In a conduction band, the well electrons are confined by a barrier of height equal to the conduction band offsets, ΔE_c.

Similarly, in the valence band, holes may be confined to discrete states in a QW of depth equal to the valence band offsets ΔE_v. The offsets and discrete states in a QW system are depicted schematically in Figure 2.4a.

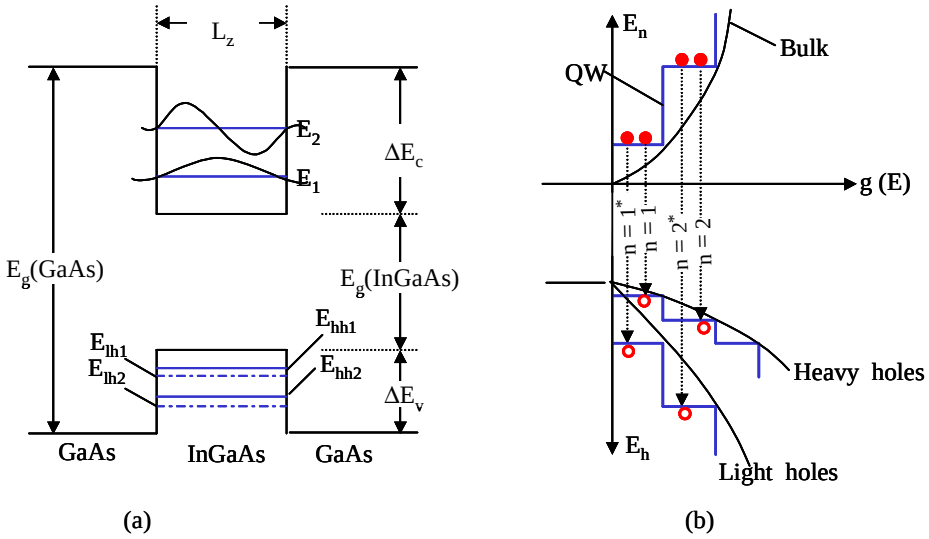

Figure 2.4 (a) Energy states in a quantum well as result of carrier confinement and **(b)** density of states and transitions for electrons E_n and holes E_h. The half parabolas that originate from the conduction band edge E_c and the valence band edge E_v correspond to the density of states for the bulk sample. The step-like densities of state are characteristic of a two-dimensional or quantum well structure and the transition of electron and holes [13].

Resulting carrier energy Eigen-values in the QW are given by

$$E(n,k_x,k_y) = E_n + \hbar^2 / 2m^*_{n,p}(k_x{}^2 + k_y{}^2) \qquad (2.3.1)$$

Where E_n is the nth confined-particle energy Eigen-value of the z component of the Hamiltonian, $m^*_{n,p}$ is the electron or hole effective mass, $\hbar$ is Planck's constant, and k_x and k_y are the unconfined x and y components of the crystal momentum. The values of E_n in (2.3.1) are designated in Figure 2.4a by E_1 and E_2 for electrons, by E_{hh1}, E_{hh2} for heavy holes, and by E_{lh1}, E_{lh2} for light holes. As shown in Figure 2.4, there are no allowed electron states below the energy E_1. Then, as shown in Figure 2.4b [13], a sub-band with a constant density of states (per unit area) $g(E)dE = \{m^*_n/(\pi\hbar^2)\}dE$ begins at E_1, followed by another sub-band (step) with a constant block of states appearing at E_2, etc. This behavior applies to holes and light holes as shown in Figure 2.4b. Figure 2.4b illustrates a very important and advantageous feature of quantum-well heterostructures: recombination can proceed from a block of electrons; all in principle located at nearly a fixed energy, say E_1. In a bulk sample, the recombining carriers are distributed in energy over parabolic

varying densities of states, which are small at the band edges, and thus in principle the electrons and holes cannot all be located at fixed energies nor that they emit in a narrow linewidth or fixed wavelength.

Thus, the quasi-two-dimensional confinement of carriers in quantum wells leads to a variety of new phenomenon, both with respect to the optical properties and the dynamics of the carriers. The electrical properties of semiconductors are dependent on the availability of holes in the valence band and electrons in the conduction states to facilitate the flow of charge under an applied potential. Similarly, optical properties arise from the electromagnetic energy absorbed or emitted as the free carriers undergo inter-band (between valence and conduction band) or inter-subband transitions.

Figure 2.4a represents a single QW structure. By fabricating many such QWs on top of each other, separated by thick layers of barriers materials, we constructed multiple quantum well MQW structure. Due to the wide barriers, no significant interaction may arise between the wave functions of confined states in adjacent wells. Consequently, the properties of MQW heterostructures are similar to those of an isolated QW of the same material and well width, and having thick barriers.

2.4 Creation of defects in QW samples: Ion implantation

High-speed optoelectronics devices rely on the short recovery times of carriers in their active region [14]. The main techniques used to achieve short carrier lifetimes in semiconductors include low-temperature (LT) epitaxial growth [15-17] and ion implantation [18-19]. LT-growth of semiconductor compounds, such as GaAs incorporates antisitic (As) point defects, which acts as carrier traps thus reducing the lifetime. Ion implantation on the other hand shortens the carrier lifetime in semiconductor materials by introducing intentional defects in the form of impurity atoms or dopants, which creates the defect states in the heterostructures. At these defect states the carriers could be trapped or recombine non-radiatively. Ion implantation is particularly attractive, mainly due to its ability to accurately control the number of implanted atoms and to place them at the desired depth of choice. Ion implantation has proven to be a viable alternative to LT-growth, and is closely controlled. A significant advantage of ion irradiation over LT-growth is the fact that once an epi-wafer is grown, the physical properties of QWs can be tailored by a choice of the energy and dose of implantation and annealing conditions. Using the ion implantation technique, the lifetime of carriers could be shortened precisely from nanoseconds (as-grown) to sub-picoseconds or even femtosecond levels by choosing the appropriate amount of irradiation dose and implantation energy [P1, P2, P3, P5, P6].

Ion implantation works by ionizing the required atoms, accelerating them in an electric field, selecting only the species of interest with an analyzing magnet and directing this beam towards the substrate. When the ions enter the substrate they continuously loose energy and change direction due to collisions with the target atoms. The depth at which the implanted atoms come to rest beneath the surface of the semiconductor depends upon:

- mass of the dopant atom
- energy of the dopant ion
- mass of the target atoms
- implantation angle
- orientation of the target
- implantation temperature

The processes responsible for slowing down (energy loss) the incoming dopant atom within the target are termed electronic and nuclear stopping [20]. Electronic stopping occurs via the excitation of the target electrons by the incoming dopant atom. It is an inelastic process and can be likened to the viscous drag experienced by a ball bearing when dropped into a jar of syrup. On the other hand, nuclear stopping, as the name suggests, is the slowing down of the incoming atom through elastic collisions between the incoming dopant atom and the target nuclei. The total energy loss or the total stopping power S [20] is defined as the loss per unit length of the ion, and is a combination of electronic and nuclear energy loss:

$$S = \left(\frac{dE}{dx}\right)_{nuclear} + \left(\frac{dE}{dx}\right)_{electronic} \qquad (2.4.1)$$

In Figure 2.5 it can be seen that at low ion velocities nuclear stopping dominates, whereas at higher velocities the energy is transferred to the electrons of the target material [21]. The deposited energy profiles in the structure could be estimated using the SRIM 2003 computer code [22].

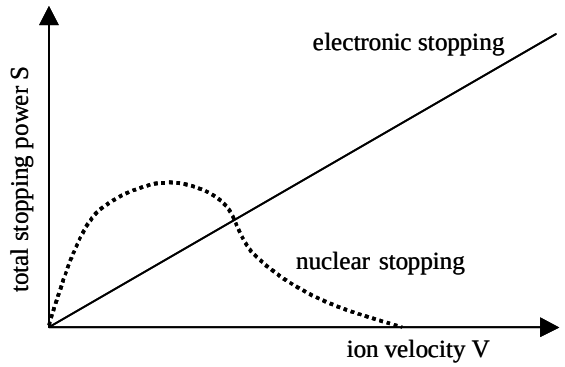

Figure 2.5 Electronic and nuclear stopping in a material [21].

Ion implantation can be further classified into light and heavy ion irradiation. It is known that heavy ion implantation of semiconductor heterostructures create mainly the cluster of point defects, while the light ion implantation create majority of isolated point defects [23-28]. The kind of defects is expected to have different effects upon the charge carrier dynamics. In this thesis we have mainly used heavy ion Ni^+ for the irradiation. However, the effect of different heavy and light ion species such as Ne^+, He^+ and H^+ ions is also investigated in detail [P6, SP3]. The energy deposited by each of these ions in the QW samples was determined entirely due to the nuclear damage [SP3].

2.5 Mode locking and semiconductor saturable absorber mirrors (SESAMs)

InGaAs/GaAs and InGaAs/InP QWs are widely used as active regions in saturable absorbers and SESAMs devices for pulse mode locking [29-34]. Typical recovery time required for pulse mode locking is about several tens of picoseconds. The recovery (decay) time of choice is achievable in these structures by proper combination of irradiation and annealing. In the following sections the basic mode locking mechanism and mode locking using the saturable absorber and SESAMs is reviewed briefly.

2.5.1 Mode locking principles

Mode locking is a method to obtain ultrashort pulses from a laser. Ultrashort light pulses are generated by locking the phases of a large number of longitudinal modes sustained by the laser gain-width [35]. A typical mode locked laser consists of the resonator with an intercavity modulator. This modulator is whether a saturable absorber, an acousto-optic, an electro-optic, or a

self-phase modulating component, modulates the amplitude or the phase of the field inside the cavity to generate short pulses. There are two broad categories of mode locking mechanism: a*ctive* and *passive*. The active mode locking uses an optical modulator controlled by an external source, *e.g.* an acousto-optic or electro-optic modulator, placed into the laser cavity to yield an ultrashort pulse [36]. Passive mode locking is performed by placing a non-liner element, *i.e.* saturable absorber in the laser cavity, which imposes an intensity-dependent loss on a light beam incident on it [37].

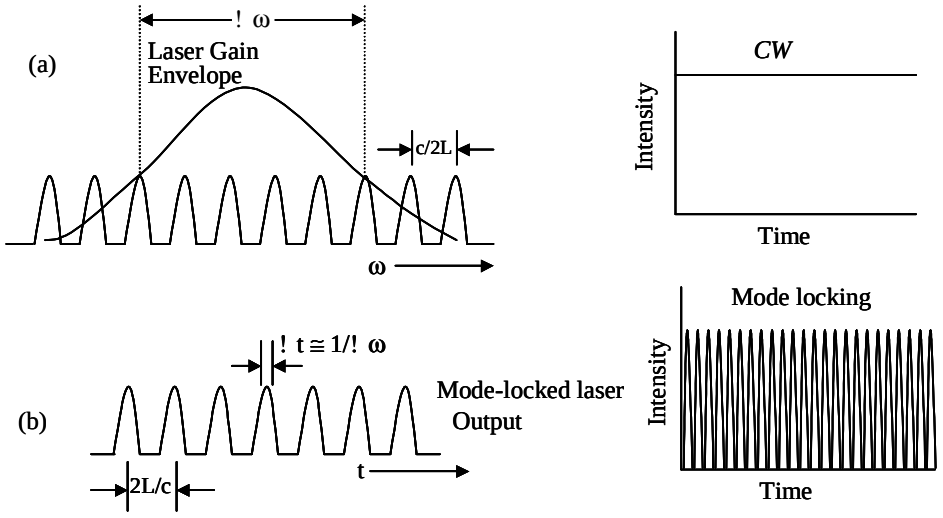

Figure 2.6 (a) The resonator modes, which oscillate, are determined by the gain profile and the resonator loss and **(b)** The temporal output of the laser with all modes locked together. In the above schematic diagram L corresponds to the cavity length of the laser.

Many modes are allowed in a laser along the resonator axis with frequency separation of *c/2L* (Figure 2.6a), where *L* is the optical length of the cavity and *c* is the speed of light. These modes usually oscillate with random phase and irregular amplitudes, resulting in a randomly time varying amplitude within the round time trip period *T=2L/c*. However, if these modes have the same phase φ, they will constructively interfere at the same instant $T_0 = (\varphi/2\pi)T$ of the round trip time. The output will thus consists of a series of pulses centered at T_0, $T_0 + T$, $T_0 + 2T$,.., (Figure 2.6) and the laser is said to be mode locked (Figure 2.6b). The lament that fixes these relative phases is referred to as mode-locker (like saturable absorbers). The width Δt of each of the successive pulses is approximately equal to the inverse of the frequency range spanned by the modes being locked in phases. In the laser resonator, mode locking in the time domain corresponds to a single pulse traveling back and forth between mirrors with loss on the output mirror being

compensated by the gain from pumping at each round trip. The operating regimes of a laser are classified on the basis of temporal characteristics of output emission. As shown in Figure 2.6, in continuous wave (CW) operation, the laser output is stationary in time, while in mode locking the output is time dependent. Other important regimes of laser operation can be found in [38].

2.5.2 Saturable absorber and SESAMs

A saturable absorber is a non-linear optical material that shows decreasing light absorption with increasing light intensity. It works like an optical switch and generate laser pulses passively through intensity-dependent absorption of the laser light. The key parameters for a saturable absorber are its wavelength range (where it absorbs), dynamic response (how fast it recovers), saturation intensity and fluence (at what intensity or pulse energy density it saturates). In particular, performance characteristics of saturable absorber depend on short recovery time of carriers in the active region and high non-linearity properties [29-34].

After an incident pulse is coupled to the absorber, upon transmission through the absorber, the low-intensity tails (wings) of the output pulse are attenuated, while the high-intensity center part of the pulse is transmitted without significant loss. As a result, the transmitted pulse has a reduced duration. When such an absorbing element is used within a laser cavity, it promotes the pulse operation with increased peak power and suppresses the lower intensity CW light. Because

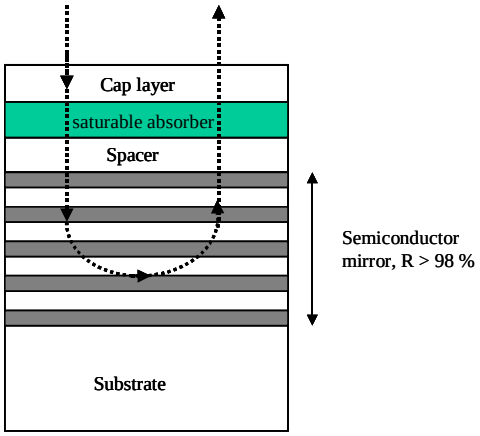

Figure 2.7 Structure of SESAM employing a saturable absorber.

the laser tends to operate with minimum cavity loss per round-trip, the longitudinal modes of the lasers become phase-locked, corresponding in time-domain to high intensity short optical pulses.

The monolithical integration of a saturable absorber with a Bragg reflector is a device known as a semiconductor saturable absorber mirror (SESAM) [29-34] and is shown in Figure 2.7. The SESAM is a saturable absorber that operates in reflection, thus the reflectivity increases with higher incoming pulse intensity. SESAMs facilitate the integration of saturable absorber into laser cavities as a cavity end mirror. It allows us to easily obtain self-starting mode locking [31]. As explained earlier, the low intensity part of the pulse will be absorbed, while the high intensity part will pass through the material with little loss, which results in compression of the pulse, *i.e.* the pulse becomes shorter and shorter when it passes through a saturable absorber. The saturable absorber shown in Figure 2.7 could either be a bulk semiconductor or QW based. The advantage of using QW based absorbing layers is that they have lower saturation energy and higher non-linearity than bulk absorbers. Increasing the volume of the absorbing layer yields higher non-linearity at the expense of increased non-saturable loss.

2.6 Femtosecond photoluminescence (PL) up-conversion technique

A schematic diagram of the basic principle of the parametric up-conversion technique [39-40] is shown in Figure 2.8. After an ultrashort pulse excites the sample, the luminescence from the sample is collected, collimated, and combined with part of the excitation pulse in a non-linear crystal such as BBO_3. The angle of the crystal is set in order to phase match the frequency of the gating pulse with a selected frequency of luminescence. A signal whose frequency is the sum of the laser and luminescence frequencies is generated by the crystal and detected by a photodetector. By varying the delay of the gating pulse and measuring the sum frequency signal, the temporal profile of the luminescence is obtained with no background signal. Since up-conversion involves virtual electronic transitions, this gate has a response time in femtosecond time scale.

(a) Instrumentation: Ti:Sapphire laser was tuned at 800 nm wavelength and the laser beam with 50 femtosecond pulses was split into two parts such that about 15% of the beam was used for the excitation (reflection from mirror M1) and the rest was used as the gate pulse. The excitation beam is focused onto a sample by lens L1 (focal length 3 cm) at incident angle close to 45^o. The excitation spot size was estimated to be roughly 30 μm. The sample emission ω_{em} is collected in a direction close to the normal of the sample surface so that the reflected excitation beam did not fall into the aperture of lens L2 and focused onto a non-linear crystal (NLC) by lens L3. The gate pulses are passed to the delay line and then focused to hit the sample emission spot on

the NLC. The crystal mixes the base, ω, and the emission, ω_{em}, frequencies and generates the sum frequency, $\omega_d = \omega + \omega_{em}$. The light intensity at ω_d is measured by the detection system. Therefore, the frequency of the detected signal is shifted up by the value ω relative to the emission frequency ω_{me} that is why the method is called up-conversion. The detection system consists of a monochromator, a photomultiplier (working in photon counting mode), a discriminator and a photon counter.

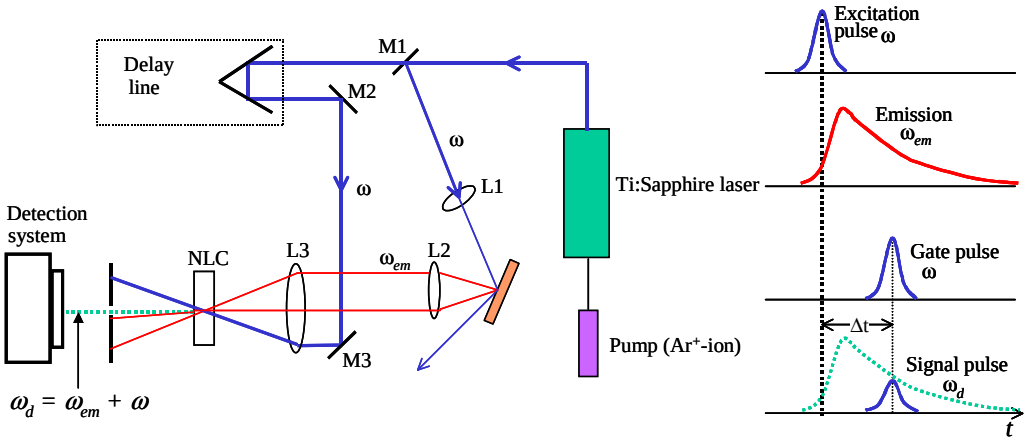

Figure 2.8 Scheme for PL up-conversion technique.

Right after mirror M1 the excitation, $I_{ex}(t)$, and gate $I_g(t)$, pulses have the same timing (and time profile). The excitation pulse at the sample is delayed by the propagation time Δt_{ex}. It creates an emission, which is given by

$$I_{em}(t) = \int_{-\infty}^{+\infty} I_{ex}(\tau) D(t-\tau) d\tau \ , \qquad (2.6.1)$$

where $D(t)$ is the sample emission response to a delta-pulse excitation *i.e.* $D(t)=0$ at $t < 0$ and $D(t) \geq 0$ *at* $t \geq 0$. The determination of the function $D(t)$ is the goal of the study. The goal of the measurement procedure is the determination of the convolution function $I_{em}(t)$. At NLC entrance the emission is delayed by time (Δt_{em}) and is given by function $I_{em}(t-\Delta t_{em})$. The delay of the gate pulse

is determined by the position of the delay line Δt_d, and by the propagation time from M1 to the delay line and from delay to NLC, Δt_g. Thus at the NLC the gate pulse is $I_g(t-\Delta t_g - \Delta t_d)$. Right after the NLC the intensity of the light at the sum frequency, ω_d, (the signal) is proportional to the product of the intensities of the gate and the emission, that is

$$I_d(t) = \eta_s I_g(t - \Delta t_g - \Delta t_d) I_{em}(t - \Delta t_{em}) \ , \qquad (2.6.2)$$

where η_s is the efficiency of the NLC. The delays Δt_{em} and Δt_g are constant. When $\Delta t_g = \Delta t_{em}$, time t can be counted from the moment of the gate pulse arrival to NLC at $\Delta t_d = 0$, and thus Equation 2.6.2 is reduced to

$$I_d(t) = \eta_s I_g(t - \Delta t_d) I_{em}(t), \qquad (2.6.3)$$

$I_d(t)$ is a short pulse with the shape determined mainly by the gate pulse since $I_{em}(t)$ is a slow function of time as compared to $I_g(t)$, in the majority of the measurements. The detection system measures energy of the pulse, *e.g.* counting photons at ω_d. Thus the measured signal is

$$U = s\int_{-\infty}^{+\infty} I_d(t)dt, \qquad (2.6.4)$$

where s is sensitivity. For a simple case of very short duration of the excitation and the gate pulses, when they can be assumed being delta-pulses, $I_g(t) = I_g\delta(t)$ and $I_{ex}(t)=I_{ex}\delta(t)$, Equation 2.6.4 leads

$$U = S\eta_s I_g I_{ex} D(\Delta t_d). \qquad (2.6.5)$$

In other words, the signal is proportional to the emission decay function at the delay time determined by the position of the delay line. Scanning the delay time one can measure the time profile of the emission decay point by point. Numeric details of various parameters are given in [41].

2.7 Pump-probe technique

In the pump-and-probe (excite-and-probe) technique an ultrashort laser pulse is separated into two pulses, the pump and the probe, with a variable optical delay between them Δt. The two incident ultrashort laser pulses are made to overlap spatially on the sample under investigation

(ideally the probe beam has to be covered completely by the excitation beam). The intense pump pulse excites the sample, causing a change in its properties. A weaker probe pulse monitors these changes initiated in the sample by the pump pulse. The time evolution of the excited state is investigated by varying the time delay between the pump and the probe pulses. The pump-probe technique may be used to investigate such properties as reflectivity, transmission, Raman scattering, and induced absorption.

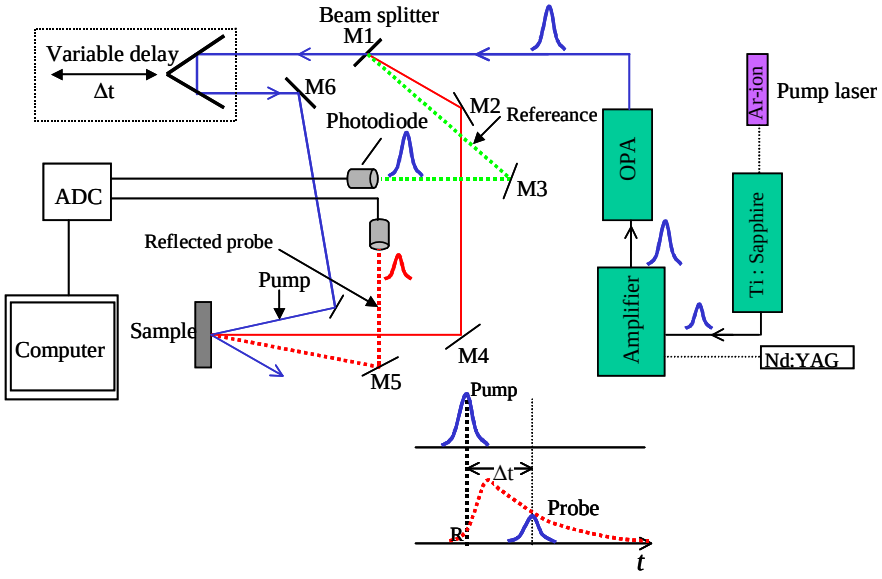

Figure 2.9 Scheme for pump-probe system.

The delay between the pump and the probe pulses on the sample can be written as

$$\Delta t = \frac{2(d_0 - d)}{c}. \qquad (2.7.1)$$

where d is the position of the reflector mirror at variable delay line and d_0 is the distance when the pump and probe reaches the sample at the same time *i.e.* setting up the zero delay.

2.8 Carrier dynamics: theoretical concepts

In III-V semiconductors, the decay of the carriers can be described by the relation [42]

$$-\frac{dn}{dt} = A_{non-rad}\, n + B_{rad}\, n^2 + Cn^3, \qquad (2.8.1)$$

where n is the carrier density, $A_{non\text{-}rad}$ is the coefficient for the non-radiative recombination due to the defects, B_{rad} is the coefficient for radiative bimolecular recombination and C is the coefficient for Auger recombination. The latter is the sum of electron-electron and hole-hole contribution and only comes into force when the carrier densities are high ($>10^{20}$ cm^{-3}) [42]. Other higher order processes may also become important at higher carrier densities. If the excitation density is not too high the term due to the Auger recombination could be neglected and Equation 2.8.1 can be written as:

$$-\frac{dn}{dt} = A_{non-rad}\, n + B_{rad}\, n^2, \qquad (2.8.2)$$

At room temperature (RT) the non-radiative recombination dominates and radiative recombination is negligible [43]. Therefore, at RT the carrier decay rate is essentially determined by non-radiative recombination:

$$-\frac{dn}{dt} = A_{non-rad}\, n\,. \qquad (2.8.3)$$

Therefore, we will not include the radiative recombination terms while describing the barrier and QW carrier dynamics at RT in the following section.

2.9 Barrier and QW carrier dynamics

Photoexcitation of the multiple quantum well structure such as InGaAs/GaAs with the excitation wavelength shorter than the barrier band gap (corresponding to the conduction and valence band gap of GaAs barrier shown in Figure 2.10) creates free carriers all over the heterostructure, *i.e.* in the barrier, QW, cap layer, and buffer. Only those carriers that reach the QW contribute to the QW carrier dynamics. The carriers, which are created far enough in the cap layer for example, and thus do not manage to reach the QW will have no influence on the QW carrier

dynamics. Further, the whole barrier's length exceeds far greater than the total QWs length, therefore majority of the photo-excited carriers are in the barriers.

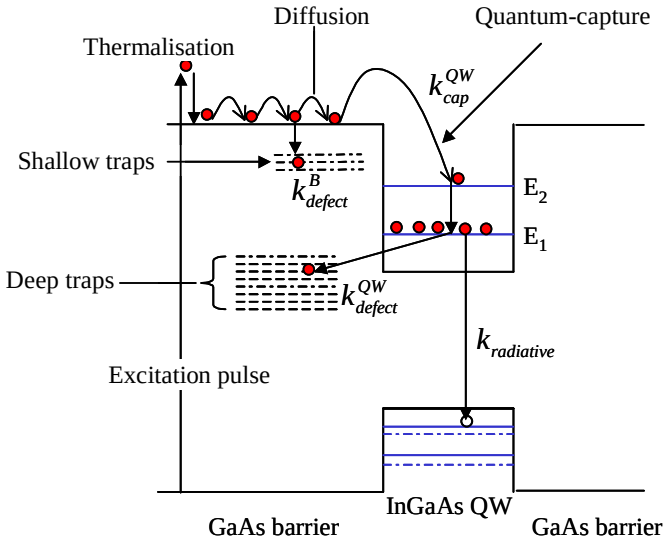

Figure 2.10 A simple mechanism for capture and decay dynamics of electrons in ion-irradiated InGaAs/GaAs QW structure upon photoexcitation.

As shown in Figure 2.10, after a very short thermalisation in the barrier, the motion of photoexcited carrier follows the following sequential steps: (1) drift and diffusion in the barrier layer, (2) quantum capture by the QW, (3) fast relaxation within the QW states (*i.e.* E_2-E_1), and finally (4) the decay of the carriers in the QW due to the non-radiative (via defects/traps states) and raditive recombinations. At RT, the radiative recombination is negligible compared to the non-radiative recombination.

Ion implantation creates defects and traps inside the heterostructure. Shallow traps denote the traps located very near to the barrier and the QW interfaces and the defects created deep enough (near the fermi level) *i.e.* far from the barrier conduction edge are denoted as deep traps (shown in Figure 2.10). Heavy ions at high implantation energies are likely to form few shallow traps and majority of deep traps. We believe that as the irradiation doses are increased, mostly the shallow traps affect the capture dynamics and that the decay dynamics is governed mainly by the deep traps [44].

If the barriers are sufficiently thin, so that the carriers are created near the vicinity of the QWs, the diffusion of carriers in the barrier layer can be neglected. According to references [45-47], if the barriers thickness is less than 20 nm, diffusion in barriers is negligible. Diffusion will play a dominant role only if the barrier thickness exceeds 50 nm. In the present work the barriers for all the samples were less than 20 nm, therefore the diffusion contribution was negligible.

The hole capture is a much faster process than the electron capture, mainly due to the large hole effective mass [48-50]. Thus, the electron dynamics will be discussed in this Thesis assuming that this is the time limiting process.

Neglecting the diffusion of carriers in the barrier layers, the decay of barrier population (N_{3D}) with time is given by:

$$\frac{dN_{3D}(t)}{dt} = -k_{cap}^{QW} N_{3D} - k_{defect}^{B} N_{3D} \ , \qquad (2.9.1)$$

where k_{cap}^{QW} is the capture or trapping rate of the carriers in the barriers by the QW and k_{defect}^{B} is the non-radiative recombination rate of carriers in the barrier layer *via* defects (native or implantation induced).

Above Equation has a trivial solution

$$N_{3D}(t) = N_0 e^{\left(k_{cap}^{QW} + k_{defect}^{B}\right)t}, \qquad (2.9.2.)$$

where N_0 is the initial population of carriers in the barrier upon photo-excitation. After the carriers are trapped by the QW and are in the lowest confined state in the QW, the decay of QW carriers with time is given by

$$\frac{dN_{QW}(t)}{dt} = \left(k_{cap}^{QW} + k_{defect}^{B}\right)N_{3D} - k_{defect}^{QW} N_{QW} \ , \qquad (2.9.3)$$

and solution of the above Equation yields

$$N_{QW}(t) = \frac{M\left(k_{cap}^{QW} + k_{defect}^{B}\right)}{k_{defect}^{QW} - \left(k_{cap}^{QW} + k_{defect}^{B}\right)}\left[e^{-\left(k_{cap}^{QW} + k_{defect}^{B}\right)t} - e^{-k_{defect}^{QW}t}\right], \qquad (2.9.4)$$

where *M* is a constant. The TRPL intensity *I(t)* is proportional to the number of carriers in the QW, therefore

$$I(t)_{PL} = \frac{N\left(k_{cap}^{QW} + k_{defect}^{B}\right)}{k_{defect}^{QW} - \left(k_{cap}^{QW} + k_{defect}^{B}\right)}\left[e^{-\left(k_{cap}^{QW} + k_{defect}^{B}\right)t} - e^{-k_{defect}^{QW}t}\right], \qquad (2.9.5)$$

where *N* is another constant. Let us define the term $\frac{1}{\tau_{cap}^{eff}} = k_{cap}^{eff} = \left(k_{cap}^{QW} + k_{defect}^{B}\right)$ as the effective capture time (or carrier lifetime in the barrier) of the carriers in the QW. Clearly the effective capture time depends upon the recombination of carriers in the barrier at the shallow defects traps. As the irradiation doses are increased the shallow traps density also increases and in turn the effective capture time is expected to decrease due to the increase in k_{defect}^{B} alone. The above term can be written as

$$I(t)_{PL} = \frac{Nk_{cap}^{eff}}{k_{defect}^{QW} - \left(k_{cap}^{eff}\right)}\left[e^{-\left(k_{cap}^{eff}\right)t} - e^{-k_{defect}^{QW}t}\right], \qquad (2.9.6)$$

or

$$I(t)_{PL} = a\left(e^{-k_{cap}^{eff}t} - e^{-k_{defect}^{QW}t}\right), \qquad (2.9.7)$$

where $a = \frac{N\left(k_{cap}^{eff}\right)}{k_{defect}^{QW} - k_{cap}^{eff}}$ and $k_{cap}^{eff} = \left(k_{cap}^{QW} + k_{defect}^{B}\right)$.

The negative term in above Equation represent the PL rise time and the positive term corresponds to the PL decay time or lifetime. Which term is negative depends, whether $k_{defect}^{QW} < k_{cap}^{eff}$ or $k_{defect}^{QW} > k_{cap}^{eff}$. In general the following conditions arise:

(1) $k_{cap}^{eff} > k_{defect}^{QW}$: In this case *a* is negative and Equation 2.9.7 can be written as

$$I(t)_{PL} = -ae^{-k_{cap}^{eff}t} + ae^{-k_{defect}^{QW}t}, \qquad (2.9.8)$$

here the first term represents the rise profile while the second term corresponds to the PL decay profile, in other words

$$I(t)_{PL} = -ae^{-\frac{t}{\tau_{rise}^{PL}}} + ae^{-\frac{t}{\tau_{decay}^{PL}}} \qquad (2.9.9)$$

The above relation holds true for the as-grown samples and samples irradiated at low doses. In this case the recombination of carriers in the barriers is negligible and

$$k_{cap}^{eff} = \left(k_{cap}^{QW} + k_{defect}^{B}\right) > k_{defect}^{QW} \text{ or } k_{cap}^{QW} > k_{defect}^{QW} \qquad (2.9.10)$$

(2) $k_{cap}^{eff} < k_{defect}^{QW}$: With the increase of the irradiation dose both the shallow and deep defects trap densities increase, but the increase in deep traps is much more pronounced, and therefore the recombination rate k_{defect}^{QW} also increases rapidly, while the recombination rate k_{cap}^{eff} increases relatively slower. For as-grown samples and the samples irradiated at low doses $k_{cap}^{eff} > k_{defect}^{QW}$, but ultimately at sufficiently high doses the condition may arise when the recombination rate of carriers at the deep centres exceeds that of the overall effective carrier capture rate by the QW *i.e.* $k_{cap}^{eff} = \left(k_{cap}^{QW} + k_{defect}^{B}\right) < k_{defect}^{QW}$. When this condition is fulfilled, *a* is positive in Equation 2.9.7, implying that the first term is positive and represents the decay profile while the second term is negative and represents the rise profile. At this point one can say that the exchange of rise and decay times take place: $\tau_{rise}^{PL} = \tau_{decay}^{PL}$ and $\tau_{decay}^{PL} = \tau_{rise}^{PL}$.

(3) $k_{cap}^{eff} = k_{defect}^{QW}$: $I(t)$ profile is no more exponential and $N_{QW}(t) = te^{kt}$.

The irradiation related damage to the crystal could be recovered partially by rapid thermal annealing (RTA). The defect dynamics is expected to be a function of annealing. The carrier capture and decay profiles are expected to depend upon the irradiation dose, type of ion species (kind of defects), implantation energy and annealing. The effect of all these parameters on the capture and decay processes has been reviewed in detail, later in this Thesis. Excellent reviews related to the capture and relaxation of carriers in semiconductor QWs structures can be found in references [57-61].

3 Results and discussion

The main heterostructure samples studied in this Thesis were, (1) InGaAs/GaAs (2) InGaAs/InP, and (3) InGa(N)As/GaAs QWs. Each of the samples were grown by solid source molecular beam epitaxy and studied by using the femtosecond time-resolved up-conversion technique.

3.1 Sample structures

(a) **InGaAs/GaAs:** samples consisted of five compressively strained QWs made of 6 nm thick $In_{0.29}Ga_{0.71}As$/17 nm GaAs heterostructures, which were deposited onto a 200 nm GaAs buffer layer on a GaAs (001) substrate and capped with a 100 nm GaAs layer.

(b) **InGaAs/InP:** samples consisted of an InP buffer layer of 100 nm thickness, deposited on an *n*-type InP substrate cut along a (100) crystal plane, followed by the growth of seven $In_{0.576}Ga_{0.424}As$/InP QWs (compressive strain ≈ 0.3% in units of lattice mismatch $\Delta a/a$), each 6 nm in thickness and separated by 8 nm thick InP barriers. The whole structure was capped with a 100 nm InP layer; all layers were nominally undoped.

(c) **InGa(N)As/GaAs:** Two $Ga_{0.63}In_{0.37}As$/GaAs QW and two $Ga_{0.63}In_{0.37}N_{0.011}As_{0.989}$/GaAs samples were grown on *n*-type GaAs (100) substrates. All samples were grown at substrate temperature T_{gr} = 420 ^{o}C or at T_{gr} = 460 ^{o}C, as read by a pyrometer. The layer structure consisted of a 100-nm thick GaAs buffer layer, a 30-nm GaAs barrier layer, 10 GaInAs (or GaInNAs) QWs each with 6 nm thickness, and a 100-nm GaAs cap layer on the top of the heterostructure.

Rapid thermal annealing (RTA) for all the samples was performed at 610 ^{0}C for 60 seconds.

3.2 Effect of excitation energy density on peak PL intensity and lifetime

We have examined the effect of the excitation energy density on the PL peak intensities and on the lifetimes for the as-grown as well as several irradiated InGaAs/GaAs and InGaAs/InP samples. The relation between the PL peak intensity and the excitation power is generally given by the relation [63]:

$$I_{PL} = \eta E_{ex}^{\gamma}, \qquad (3.2.1)$$

where I_{PL} denotes the peak PL intensity, η represents the PL efficiency including the capture, ionization, and recombination processes of the carriers, E_{ex} is the excitation power and γ describes the parameter determined by the radiative recombination mechanism. If the value of $\gamma \leq 1$, the dominant recombination mechanism for the radiative transitions is dominated by trapped excitons, while for values γ>1 the main mode of radiative recombination is due to the free carriers [63].

In our experiments steady state PL peak intensity (Figure 3.1) as well as peak TRPL intensity (Figure 3.2) show nearly a linear dependence on the excitation intensity. Linear dependence ($\gamma \approx 1$) means that the dominant mechanism of radiative recombination at RT is excitonic rather than the free carriers. It should be noted, that the non-radiative recombination prevails at RT so that the radiative recombination is negligible and the main mechanism of radiative recombination at RT is excitonic.

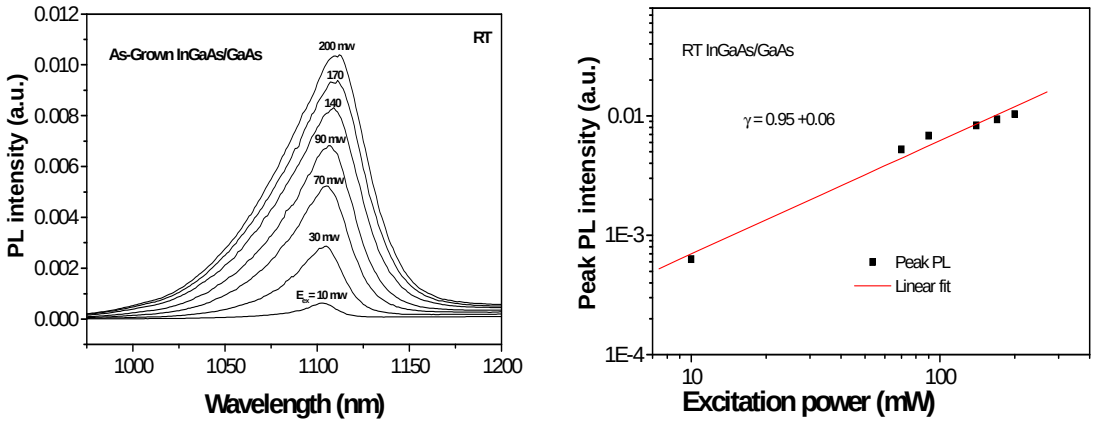

Figure 3.1 Dependence of PL peak intensity on the excitation power.

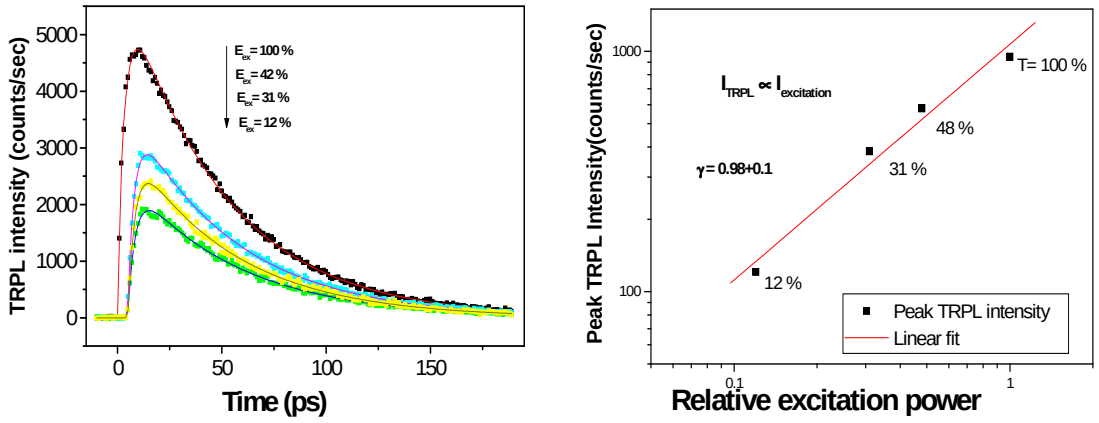

Figure 3.2 Dependence of peak TRPL intensity on the relative excitation power.

At the same time, the decay time was found to be independent of the excitation intensity. The decay profiles for the sample irradiated at 10×10^{10} ions cm^{-2} when excited at different intensities are shown in Figure 3.2. As the excitation intensity decreases when filters are used, the TRPL intensity also decreases, but the lifetimes (slopes in Figure 3.2) remain essentially the same. Independence of the lifetime on the excitation intensity indicates that the radiative decay is due to the monomolecular recombination and for the excitation density used throughout in this Thesis; the energy states in the QWs were not saturated.

3.3 Capture and decay of carriers in InGaAs/GaAs quantum wells

InGaAs QWs are widely used in high-speed optoelectronics devices as the active region. In particular, the performance characteristics of InGaAs QWs for optical switches and semiconductor saturable absorber mirrors depend on QWs recovery time. In the following sections the effects of various parameters on capture and decay dynamics are investigated in detail.

3.3.1 Effect of Ni^+-irradiation and RTA

InGaAs/GaAs QWs samples were irradiated by 10 MeV Ni^+ with doses ranging from 1 to 50×10^{10} ions cm^{-2}. The photo-excitation of the sample with 50 fs pulses creates non-equilibrium carriers, mainly in the GaAs barriers, from where the carrier transport occurs to the QWs. The formation or rise profiles of the carriers in the QWs irradiated at different doses are shown in Figure 3.3a. In a few ps time scale the PL intensity rises from zero to its maximum value indicating a rise in the population of carriers in the QWs. The PL intensity decreases systematically as the dose is increased but the profiles remain exponential at all doses. The observed exponential nature of the PL formation suggests that the time-limiting step in filling the QW states is not diffusion of the carriers from the barriers, but trapping (capture) by the QW. In other words the QW collects only those carriers, which are formed relatively near the well, and that the electron-hole pairs generated far from the QW interfaces never reach the well as they recombine non-radiatively at the irradiation induced defect centers.

Since the experimentally calculated rise time depends both on the diffusion and the effective capture (capture at the defect states and by the QW) of carriers, the rise time in the absence of the diffusion is approximately due to the direct capture by the QW and the capture at the shallow defects. For the as-grown sample and the sample irradiated at low doses the recombination

at the shallow defects is negligible, therefore the rise time is mainly determined by the direct carrier capture by the QW. At high doses the shallow defect density increases, which results in enhanced recombination at the defect sites. The effective capture time decreases as the irradiation dose increases (Table 3.2.1). For the as-grown QW the capture time is about 6 ps but for the sample irradiated at the highest dose of 50×10^{10} ions cm^{-2}, the QW relaxation time is 0.62 ps.

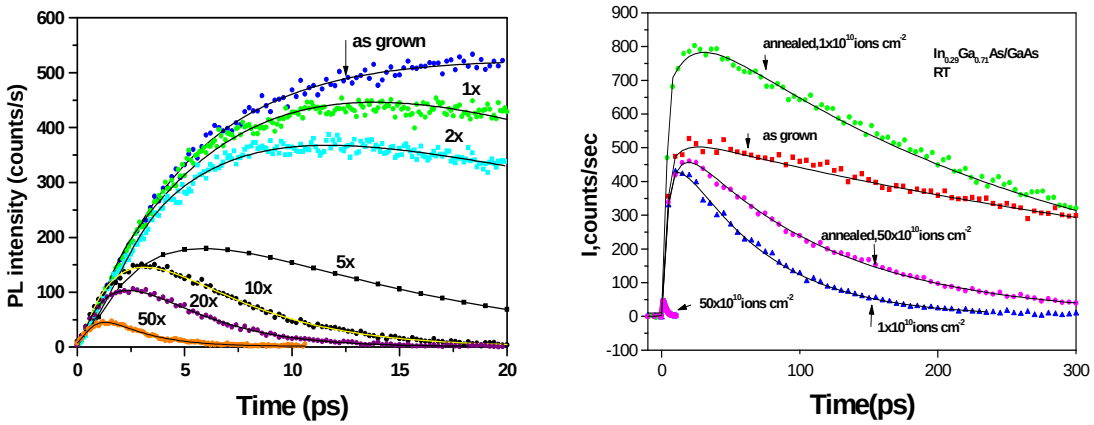

(a) (b)

Figure 3.3 (a) TRPL rise profiles of carriers in InGaAs/GaAs exposed to different Ni^+ doses (indicated in 10^{10} ions cm^{-2}) and **(b)** effect of irradiation and post-annealing on TRPL decay profiles of few selected samples.

The decrease in the PL rise time with irradiation dose is due to the increase of carrier recombination at the shallow defects traps located near the barrier and QW region (as shown in Figure 2.10). The effective capture time for the as-grown and the irradiated samples after RTA is nearly constant, about 4.5 ps, independent of the irradiation dose (Table 3.1). For the highest irradiated sample the effective capture time increases from 2 ps to 4.4 ps after RTA. This can be understood accounting for the fact that the annealing at 600 ^{0}C for 60 sec. removes few shallow traps, especially for the samples irradiated at higher doses.

Ni^+-irradiation is very effective in achieving the sub-picosecond lifetimes in the InGaAs/GaAs samples. The QW decay profiles for selected irradiated and irradiated-annealed samples are shown in Figure 3.3b. The decay profiles are mono-exponential for the irradiated and irradiated-annealed samples. The PL intensity and the slopes decrease rapidly as the Ni^+ dose increases. The carrier barrier QW lifetimes for the entire dose regimes are plotted in Figure 3.4. The QW lifetime is 460 ps for the as-grown sample and only 0.62 ps for the highest irradiated sample. Table 3.1 shows the carrier barrier lifetime of 2 ps at the highest dose, as obtained using

Equation 2.9.9 from the data fitting. As was discussed in Section 2.9, at higher doses the assignment of the rise and decay time values is not straightforward and depends on the condition whether $k_{cap}^{eff} < k_{defect}^{QW}$ or $k_{cap}^{eff} > k_{defect}^{QW}$. At doses 20×10^{10} and 50×10^{10} ions cm^{-2}, $k_{cap}^{eff} < k_{defect}^{QW}$, therefore the rise and decay time values extracted from Equation 2.9.9 are assigned vice-versa. The details can be found in [P1]. The short lifetimes are the result of the creation of a large number of induced deep defect states (Figure 2.10), which acts as non-radiative recombination and trapping sites for the carriers in the QW. Thus sub-picosecond lifetimes could be achieved in InGaAs/GaAs QWs samples by irradiation with heavy ion Ni^{+}.

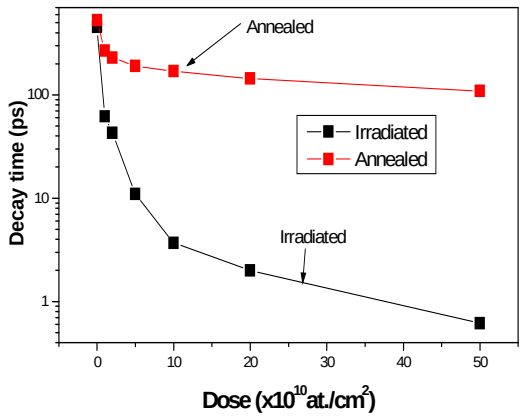

Figure 3.4 Decay time for Ni^{+}-irradiated and annealed InGaAs/GaAs QWs.

The optical quality of the sample degrades due to the irradiation damage. It could be recovered partially by annealing. The effect of RTA on the decay time is shown in Figure 3.4. The lifetime of the as-grown QW sample is not much affected by RTA, it increases only from 460 to 530 ps. The as-grown QWs are likely to contain misfit dislocations due to the high lattice mismatch between InGaAs and GaAs layers [62]. RTA at 610 ^{0}C for 60 s is therefore unable to remove most of these defects. For irradiated samples, RTA removes the defects substantially: decay time for the lowest irradiated sample increases from 62 ps to about 270 ps, while for the highest irradiated sample RTA improves the lifetime remarkably from 0.6 ps to 109 ps. RTA removes mainly the deep traps, which is confirmed by the increase in the decay time after the annealing, while annealing is not able to remove the shallow traps near the barrier and QW region, this is confirmed by the fact that annealing increases the decay time significantly and has only a mild effect on the effective capture time. Thus we have shown that with a proper combination of Ni^{+}-irradiation and RTA one could achieve precisely the desired recovery time in InGaAs/GaAs

samples. The details of barrier and QW lifetimes for irradiated and irradiated-annealed samples are compiled in Table 3.1.

Table 3.1 Barrier and QW lifetimes of Ni^+-irradiated and annealed InGaAs/GaAs QWs.

Ni^+ dose (ions cm^{-2})	Irradiated		Annealed	
	$\tau_{barrier}$	τ_{QW}	$\tau_{barrier}$	τ_{QW}
0	5.7 ± 1.3	460 ± 25	4.7 ± 0.5	530 ± 30
1×10^{10}	4.6 ± 0.2	62 ± 3	4.2 ± 0.5	269 ± 14
2×10^{10}	5.0 ± 1.0	43 ±2	4.4 ± 0.6	230 ± 15
5×10^{10}	3.0 ± 0.3	11 ± 0.8	3.3 ± 0.4	190 ± 10
10×10^{10}	2.5 ± 0.2	3.7 ± 0.3	4.5 ± 0.7	170 ± 8
20×10^{10}	2.4 ± 0.4	2 ± 0.2	4 ± 0.3	144 ± 7
50×10^{10}	2 ±0.3	0.62 ±0.1	4.4 ± 0.4	109 ± 6

3.3.2 Thermal instability of defects: room temperature ageing

One of the major highlights of the results obtained in this Thesis is the observation that Ni^+-irradiated defects are not thermally stable during certain time period after the irradiation.

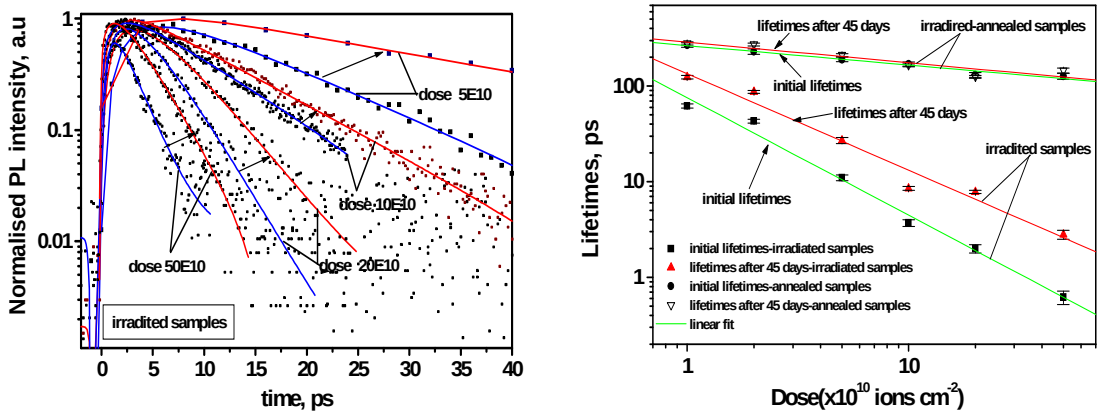

(a) (b)

Figure 3.5 (a) Selected TRPL decay profiles of Ni^+-irradiated InGaAs/GaAs QW samples. The decay profiles in red lines indicate the changes when the experiments were repeated after a gap of 45 days and **(b)** effect of ageing on decay time in Ni^+-irradiated and annealed QWs. A two-fold increase of the lifetimes is seen in Ni^+- irradiated samples after 45 days from the initial measurements. Lifetimes after 60 and 100 days of ageing were similar to that for 45 days and are not shown here for clarity.

Surprisingly, it was observed that the decay time of the fresh sample increased by two-fold when the TRPL measurements were repeated 45 days after the initial lifetime measurements (Figure 3.5). Repetition of the experiments after 60 and 100 days duration shows no more increment in lifetimes. Thus, after the irradiation the defects are removed till a particular time,

such that half of the defects are removed and thereafter the samples remain stable with no further changes. The time period when the defects are unstable is approximately 30 days from the irradiation. We call this phenomenon a room temperature self-annealing of defects or the ageing process. On the other hand, the defects were stable with time for the annealed samples and no changes in their lifetime were observed after the irradiation.

These results are crucial for the device designers as the change in the recovery time could make the device having unpredictable results in longer terms.

3.3.3 Effect of ion implantation energy

In addition to the ion implantation dose, the decay time also depends upon the implantation energy. Figure 3.6a shows the dependence of decay time for InGaAs/GaAs QWs samples on the implantation energy at a fixed dose of 5×10^{10} ions cm^{-2}. The implantation energies were varied from 6 to 30 MeV.

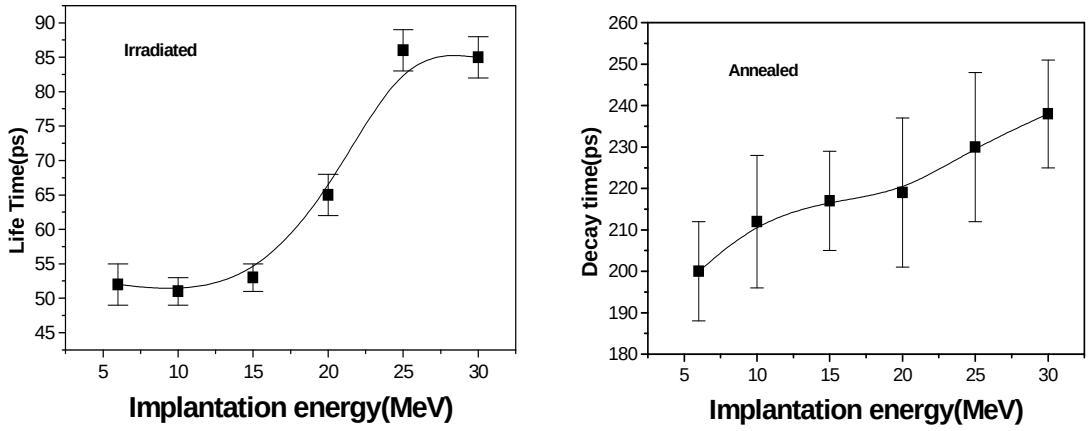

(a) (b)

Figure 3.6 Variation of decay time with the implantation energy in InGaAs/GaAs QW sample at a fixed Ni^{+} dose of 5×10^{10} ions cm^{-2} **(a)** before annealing and **(b)** after annealing.

As can be seen in the Figure 3.6, the decay time increases from 52 to 85 ps as the implantation energy increases from 6 to 30 MeV. This is due to the fact that with the increasing implantation energies the amount of nuclear deposited energy in the active region decreases. At high implantation energies ions get implanted deep inside GaAs substrates causing less damage than the low energy ions but leaves trails of defects along their trajectory in the top layers. The defects may have a higher capture rate (midgap states) but only have a small density per unit

surface in each QW. This explains the increase in decay time with implantation energies. From Figure 3.6, it is clear that for efficient defect production, the ions with implantation energy ≤ 15 MeV are preferred.

The decay time values after the annealing are shown in Figure 3.6b. Decay time depends on the annealing and increases from 52 to 200 ps for the sample implanted at 6 MeV, while the increment is from 85 to 238 ps for the sample irradiated at 30 MeV. However, the capture time does not depend on either the implantation energy or the annealing after the ion implantation. The capture time is about 2.5 ps for all the samples. The rise and decay time values as a function of the implantation energy is given in Table 3.2.

Table 3.2 TRPL rise and decay time values *vs.* the implantation energy for InGaAs/GaAs QWs at a fixed Ni^+ dose of 5×10^{10} ions cm^{-2}, before and after the annealing.

Implantation energy (MeV)	Before annealing		After annealing	
	τ_{rise}	τ_{decay}	τ_{rise}	τ_{decay}
6	2.1 ± 0.2	52 ± 3	2.1 ± 0.1	200 ± 12
10	2.0 ± 0.1	51 ± 2	2.8 ± 0.5	212 ± 16
15	1.7 ± 0.1	53 ± 2	2.3 ± 0.5	217 ± 12
20	2.2 ± 0.2	65 ± 3	2.9 ± 0.4	219 ± 18
25	2.7 ± 0.4	86 ± 3	2.5 ± 0.2	230 ± 18
30	2.4 ±0.3	85 ± 3	2.4 ±0.1	238 ± 13

3.3.4 Effect of light and heavy ion-irradiation

The effect of different heavy (Ni^+ and Ne^+) and light (He^+ and H^+) ions irradiation on the capture and decay dynamics in InGaAs/GaAs QWs was studied in detail. The implantation energy for each of the ions were chosen such that they have about the same stooping range profile in the sample and each of the ions pass through the active region. The implantation energies used for H^+, He^+, Ne^+, and Ni^+ were 100 keV, 200 keV, 500 keV, and 6 MeV respectively.

The main results obtained from these experiments are: the effective capture time for the light ions He^+ and H^+ is almost independent of the irradiation dose, while for the heavy ions, Ne^+ and Ni^+, the capture time decreases with the dose (Figure 3.7a). The fastest population of the carriers in the QW was observed for the Ne^+ ion irradiation, with the effective capture time of only 1 ps. The capture time for light ions is about 3.5 ps (Figure 3.7a). Irradiation with light ions is as effective as

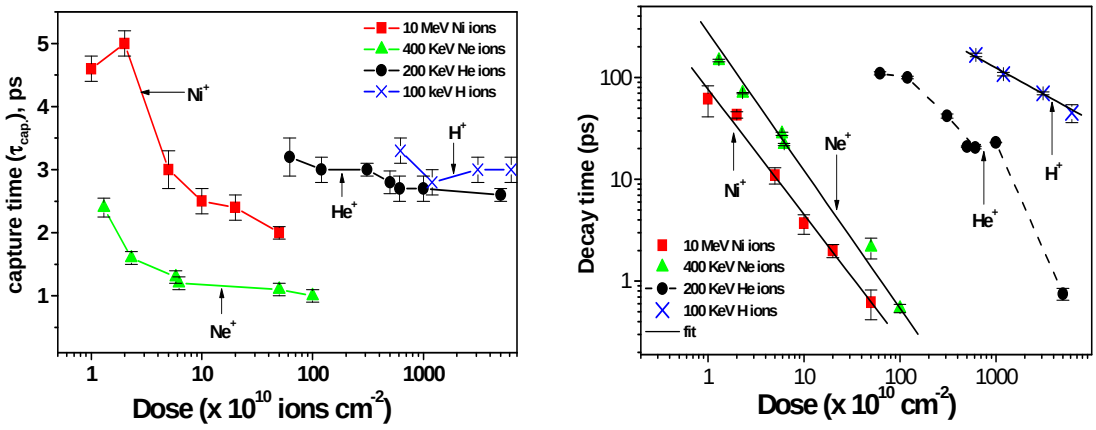

(a) (b)

Figure 3.7 InGaAs/GaAs QWs irradiated with heavy (Ni^+, Ne^+) and light (He^+ and H^+) ions **(a)** capture time as a function of irradiation dose and **(b)** decay time as a function irradiation dose

that with heavy ions in achieving the desired short decay time (Figure 3.7b) but for similar nuclear energy deposition and penetration depth profiles for each ion species, much higher doses are required for lighter ions implantation than that for Ne^+ and Ni^+ to yield the same carrier lifetime.

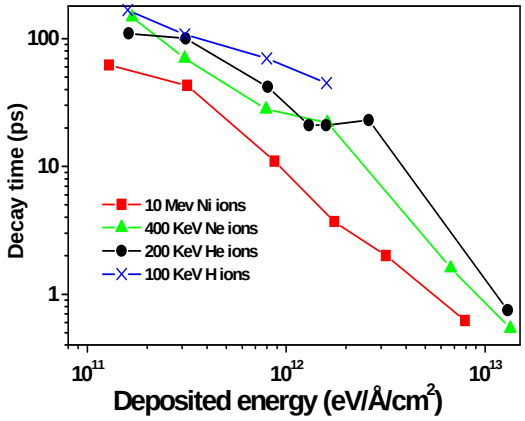

Figure 3.8 Decay time as a function of deposited energy for different light and heavy ions. Different decay times are observed for similar nuclear deposited energy.

Figure 3.8 shows the decay time values for each ion as a function of the nuclear deposited energy in the active region. For similar nuclear deposited energy, each irradiation resulted in different decay time values. This suggests that decay time depends not only on the deposited energy but also on the specific kind of defects the different ions produce. It is known that light ions

create mainly isolated point defects, while the heavier ions produce a cluster of defects. While comparing the Ni^+ an Ne^+-irradiation, it is clear from Figure 3.7, that the carrier lifetime and the doses were about the same for both the methods but, Ne^+ ions are preferred over Ni^+ due to the faster capture dynamics, remarkably lower implantation energy requirement and low cost of process (Ne^+ being a noble gas) to obtain the desired irradiation induced effects.

3.4 Capture and decay of carriers in InGaAs/InP quantum wells

3.4.1 Effect of Ni^+-irradiation and RTA

The effect of Ni^+-irradiation and post-annealing on the carrier capture and decay process was investigated in InGaAs/InP QWs structures. The effective capture time decreases with the dose, being 8 ps for the as-grown (no irradiation) sample and 2 ps for the sample irradiated at the highest dose of 50×10^{10} ions cm^{-2} (Figure 3.9a). Annealing has no effect on the capture time.

Since annealing affects the decay time (Figure 3.9 b) significantly, but not the capture time, it can be argued that the defects responsible for bringing change in the carrier capture dynamics are different from those affecting the decay time. This means that the shallow defects produced near

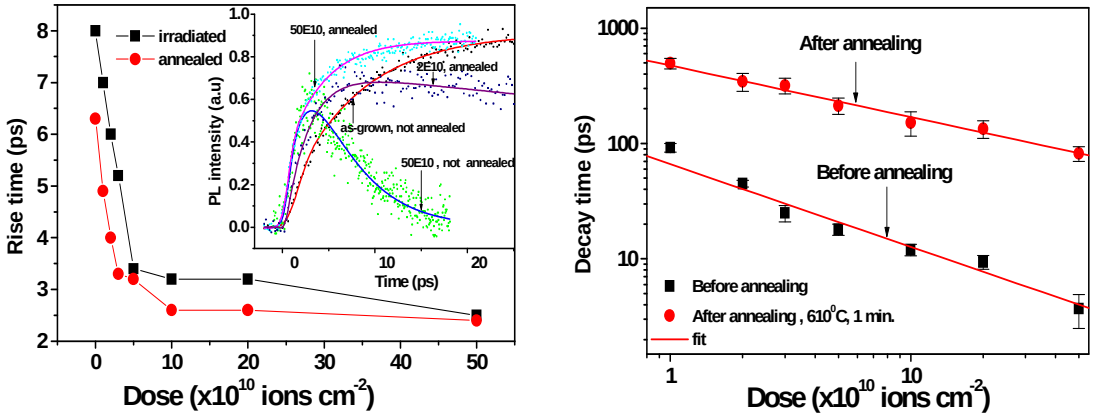

(a) (b)

Figure 3.9 (a) PL rise time (≈ capture time) for irradiated and irradiated-annealed InGaAs/InP samples as a function of Ni^+ dose and **(b)** decay times of irradiated and subsequently annealed InGaAs/InP QWs as a function of Ni^+ dose.

the barrier and QW interfaces or in and around barriers only affect the capture time while the deep traps do not significantly effect the capture dynamics because the electron wave function is delocalized for the shallow centers while it is localized compared to the deep traps. Thus most likely the electrons in the barrier deal with the shallow traps while their transfer to the QW. The

deep defect states are responsible for shortening the QW decay time alone. The decay time decreases rapidly as the dose increases (Figure 3.9b). For the as-grown QW, the decay time is 1.19 ns, while it is only 3.7 ps for the highest irradiated sample. Annealing brings no change in the as-grown sample, while it recovers defects to some extent in irradiated sample, but not completely.

Figure 3.10a shows the steady state PL intensities as a function of the irradiation dose. The steady state PL intensity decreases rapidly as the dose increases. This correlates well with the TRPL decay curves showing the rapid decrease in the lifetimes and TRPL intensities (Figure 3.9). Annealing recovers the defects only partially. Figure 3.10b shows the XRD patterns of as-grown sample and the sample irradiated at doses of 1×10^{10}, 10×10^{10}, and 50×10^{10} ions cm^{-2}. The difference in the SL satellite peaks on both sides of the main peak suggests that small structural changes take place at higher doses. Some changes in the composition of Ga in the barriers and in the wells are also possible due to a small amount of intermixing at higher doses. These small changes in the composition may accelerate the carriers trapping by the QW and might affect the capture dynamics.

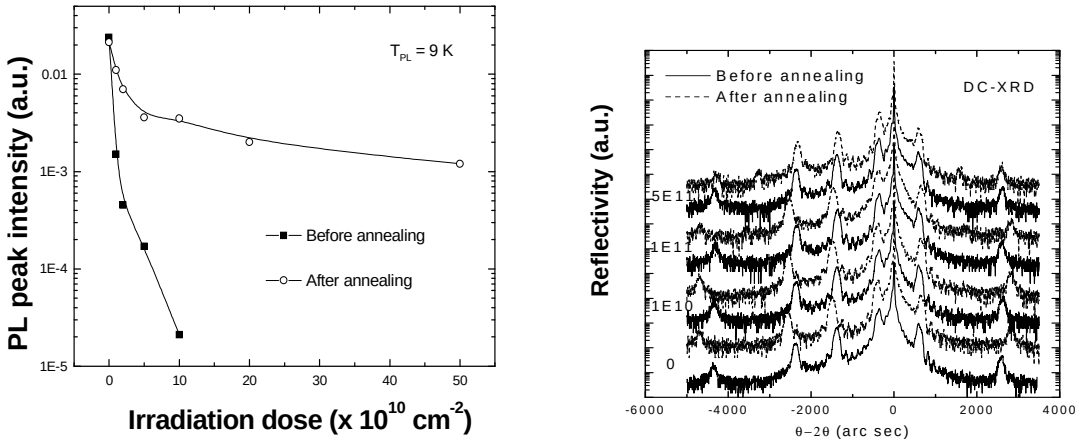

(a) (b)

Figure 3.10 (a) Low temperature PL peak intensities as a function of the irradiation dose and **(b)** XRD rocking curves for the as-grown and the samples irradiated at different doses, before and after the annealing.

The rise and decay time values for the Ni^{+}-irradiated and post irradiated annealed samples are compiled in Table 3.3.

Table 3.3 TRPL rise and decay time values for Ni^+-irradiated and annealed InGaAs/InP QWs.

Ni^+ dose (ions cm^{-2})	Irradiated		Annealed	
	τ_{rise}	τ_{decay}	τ_{rise}	τ_{decay}
0	8±1.4	1186±135	6.3±2	946±252
1×10^{10}	7±1	92±8	4.9±1.3	496±52
2×10^{10}	6±0.6	45±3	4±0.9	345±61
3×10^{10}	5.2±1.4	25±3	3.3±0.8	318±49
5×10^{10}	3.4±0.8	18±2	3.2±1.1	213±34
10×10^{10}	3.2±0.9	12±1.4	2.6±0.9	152±36
20×10^{10}	3.2±0.9	9.4±1.3	2.6±0.7	134±23
50×10^{10}	2.5±0.87	3.7±1.2	2.4±0.7	82±12

3.4.2 Effect of ion implantation energy

Figure 3.11 illustrates the decay times for the QWs irradiated at $\phi = 5 \times 10^{10}$ ions cm^{-2} for the implantation energies between 6 MeV and 30 MeV.

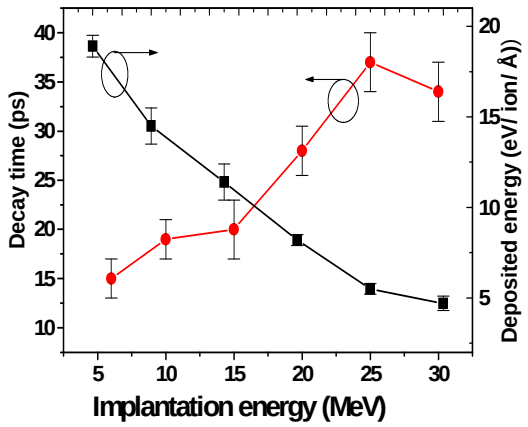

Figure 3.11 Decay time and deposited energy in the active region of InGaAs/InP QWs structure irradiated at 5×10^{10} ions cm^{-2} Ni^+ dose, as a function of implantation energy.

The τ_{decay} increase systematically from 15 ps to 37 ps in the energy range from 6 to 25 MeV. This behaviour can be understood in terms of the nuclear deposited energy (in units of eV/ion/Å), since the damage produced in InP and GaAs is dominated by nuclear collision processes for ions in this range [64] (track formation becomes significant only at higher electronic deposition [65]).

The nuclear deposited energy in the active region was determined using the SRIM2003 computer code [22] by calculating the energy transferred to recoil by the incoming ion in the active region in the depth range of 100 to 200 nm. The result was averaged over the InP and InGaAs multiplayer parts (below the top 100 nm InP layer) and is given in Figure 3.11. The results reveal that the nuclear deposited energy decreases with increasing implantation energy, and this trend is almost exactly opposite to the change in lifetime. Less damage is correlated with longer lifetimes. Accordingly, in order to effectively produce defects, low implantation energies (less than 5 MeV for Ni^{+}) are preferred.

3.5 Dynamics of GaIn(N)As/GaAs QWs

Effects of the MBE growth temperature and rapid thermal annealing (RTA) on the PL rise and decay dynamics of carriers in $Ga_{0.63}In_{0.37}As/GaAs$ and $Ga_{0.63}In_{0.37}N_{0.011}As_{0.989}$ / GaAs quantum well samples was investigated. The GaInAs/GaAs quantum wells, grown at temperatures (T_{gr}) of 420 ^{o}C and 460 ^{o}C, exhibited similar PL rise times of carriers of about 3.5 ps. RTA at 610 ^{o}C for 60 seconds had no significant effect on the rise time. On the other hand, the decay time depended on T_{gr}, increasing from 439 ps to 517 ps for the sample grown at T_{gr} = 420 ^{o}C and T_{gr} = 460 ^{o}C respectively.

Alloying 1.1 at-% nitrogen with GaInAs strongly influenced the carrier dynamics. The PL rise and decay times for the GaInNAs / GaAs sample were about 1.0 ps and 11 ps, respectively, when grown at 420 ^{o}C, and 1.0 ps and 15 ps for the sample grown at 460 ^{o}C. Incorporation of N creates additional defect centers in the heterostructure. Shorter PL rise time observed in N containing samples is due to the trapping of carries by the defect states near the barrier layer rather than the fast capture of electrons by the QW. This is confirmed by about a 107 times quenching in the steady state PL intensity (Table 3.4) and only about 40 times decrease in the decay time after the incorporation of N for T_{gr} = 420 ^{o}C sample.

RTA reduced the amount of structural defects particularly for the lower growth T_{gr} = 420 ^{o}C sample, which indicated the carrier lifetime of 70 ps upon RTA treatment. For the T_{gr} = 460 ^{o}C sample the lifetime was only 40 ps after RTA. The longer lifetime recovery for the low-T_{gr} sample suggested that low T_{gr} should be favored over high T_{gr} if the sample is subjected to post-growth RTA. The numeric details of the rise and decay time values for different samples are compiled in Table 3.4.

Table 3.4 TRPL rise (effective capture) times, decay times and PL intensity for $Ga_{0.63}In_{0.37}As/GaAs$ and $Ga_{0.63}In_{0.37}N_{0.011}As_{0.989}/GaAs$ QWs grown at different growth temperatures (T_{gr}), before and after the annealing.

Sample	T_{gr}	As-grown		Annealed		As-grown
	(^oC)	Rise (ps)	Decay (ps)	Rise (ps)	Decay (ps)	PL intensity (a.u.)
GaInAs/GaAs	420	3.1±0.2	439±14	3.2±0.4	434±12	2.362
GaInAs/GaAs	460	3.5±0.4	517±16	3.3±0.6	553±19	3.775
GaInNAs/GaAs	420	1±0.1	11±0.8	1.8±0.2	68±6	0.022
GaInNAs/GaAs	460	1±0.1	15±1.3	1.4±0.2	40±4	0.024

In summary, the incorporation of N in GaInAs could be an alternative to the ion irradiation to achieve short lifetimes. Furthermore, for GaInAs samples, lower the growth temperature, the smaller the decay time. For GaInNAs samples the growth temperature should be low enough to recover more defects after the RTA.

4. Conclusions

Carrier dynamics have been investigated in MBE grown InGaAs/GaAs, InGaAs/InP, and InGa(N)As/GaAs QW structures. The aim was to make these semiconductor structures faster for ultrafast operation by incorporating the defects using the ion implantation technique and to study the effect of different parameters such as irradiation dose, ion species, implantation energy, MBE growth temperature, and annealing on the carrier transport and relaxation processes. The main results obtained are summarized below

(1) The decay time could be reduced to sub-picoseconds levels in InGaAs/GaAs and InGaAs/InP QW structures via Ni^+-irradiation. Annealing was found to increase the lifetime substantially in all the irradiated structures. By appropriate combination of irradiation and annealing, the desired decay times of choice are achievable in these structures.

(2) The defects created by Ni^+-irradiation are not stable for a certain period of time after the implantation. The decay time was found to increase two-fold when the measurements were repeated after a gap of 30, 45, and 100 days after the initial measurements of fresh irradiated samples. The defects in annealed samples were found to be stable with time.

(3) In general, the effective capture time decrease with the irradiation dose, while annealing has no effect on it. Ion implantation creates few shallow traps and a majority of deep traps in heterostructures. The capture dynamics is affected mainly by the shallow traps while the decay dynamics is affected mainly by the deep traps.

(4) For lighter ions (He^+ and H^+) capture time is almost insensitive to the irradiation dose while for the heavier ions (Ni^+ and Ne^+) it decreases as the doses are increased. Either of the light and heavy ions is capable of achieving sub-picosecond lifetimes in InGaAs/GaAs samples. However for similar nuclear deposited energy and penetration depth profile, irradiation with Ne^+ requires far less implantation energy than Ni^+ to achieve the same irradiation induced effects. Irradiation with Ne^+ was found to be a good alternative to Ni^+.

(5) For InGaAs/GaAs QWs the decay time increase with the MBE growth temperature. Incorporation of N has a tremendous effect on the charge carrier dynamics. The decay time is reduced to about 11 ps from 439 ps after N incorporation. Interestingly, the effect of annealing was more pronounced for the sample grown at lower growth temperature.

References

[1] J. Shah, “Ultrafast spectroscopy of semiconductors and semiconductor nanostructures”, Springer, Berlin, 1996.

[2] R. R. Alfano, “Semiconductors Probed by Ultrafast Laser Spectroscopy”, Volumes I and II, Academic, New York, 1984.

[3] J. Shah, “Hot carriers in semiconductor nanostructures: Physics and applications”, Academic Press, Boston, 1992.

[4] J. Singh, “Electronic and optoelectronic properties of semiconductor structures”, Cambridge University Press, 2003.

[5] J. Singh, “Semiconductor optoelectronics: physics and technology”, McGraw-Hill International, New York, 1995.

[6] S. Adachi, “ Physical properties of III-V semiconductor compounds”, Wiley-VCH, 1992.

[7] R. E. Nahory, M. A. Pollack, W. D. Johnston and R. L. Barns, “Band gap versus composition and demonstration of Vegard’s law for $In1\text{-}xGa_xAs_yP_{1-y}$ lattice matched to InP”, Appl. Phys. Lett., vol. 33, p. 659, 1978.

[8] A. Y. Cho, “The technology and physics of molecular beam epitaxy”, . in: C. H. C. Parker (Ed.) vol.1, Plenum Press, New York, NY, 1985.

[9] V. A. Shchukin, N. N. Ledentsov and D. Bimberg, “Epitaxy of nanostructures”, Springer Berlin, 2003.

[10] V. N. Lutskii, “Quantum size effect-present state and perspectives of experimental investigation”, Phys. Status Solidi (a), vol. 1, p.199, 1970.

[11] M. I. Elinson, V. A. Volkov, N. N. Lutskii and T. N. Pinsker, “Quantum size effect and perspectives of its practical applications”, Thin Solid Films, vol. 12, p. 383, 1972.

[12] R. Dingle, “Confined carrier quantum steps in ultrathin semiconductor heterostructures”, in Festkorper probleme XV (Advances in Solid State Physics), H. J. Queisser(Ed.) New York, Pergamon, , p. 21, 1975.

[13] N. Holonyak, R. M. Kolbas, R.D. Dupuis and P. D. Dapkus, “Quantum-well hetrostructures lasers”, IEEE. J. Quantum Electron., vol. QE-16, p. 170, 1980.

[14] J. Singh. “Semiconductor optoelectronics: physics and technology”, McGraw-Hill International, New York, 1995.

[15] C. Baker I. S. Gregory, W. R. Tribe, I. V. Bradley M. J. Evans, E. H. Linfield and M. Missous, “Highly resistive annealed low-temperature-grown InGaAs with sub-500 fs carrier lifetimes”, Appl. Phys. Lett., vol. 85 , p. 4965, 2004.

[16] R. A. Metzger, A. S. Brown, L. G. Mcray and J. A. Henige , J. Vac. Sci. Technol. B, vol. 11, p. 798, 1993.

[17] Y. Chen, S. S. Prabhu, S. E. Ralph and D. T. McLnturff, "Trapping and recombination dynamics of low-temperature-grown InGaAs/InAlAs multiple quantum wells", Appl. Phys. Lett., vol. 72, p. 439, 1998.

[18] M. B. Johnson, T. C. McGill and N. G. Paulter, "Carrier lifetimes in ion-damaged GaAs", Appl. Phys. Lett., vol. 54, p. 2424, 1989.

[19] M. Lambsdorff, J. Kuhl, J. Rosenzweig, A. Axmann and J. Schneider, "Subpicosecond carrier lifetimes in radiation damaged GaAs", Appl. Phys. Lett., vol. 58, p. 1881, 1999.

[20] J. F. Ziegler, J. P. Biersack and U. Littmark, "The Stooping And Range Of Ions In matter", Pergamon New York, 1985.

[21] K. Schwartz, C. Traumann and R. Neumann, "Electronic excitations and heavy-ion-induced processes in ionic crystals", Nucl. Instr. Meth. Phys. Res. B, vol. 209, p. 73, 2003.

[22] J. F. Ziegler SRIM-2003 Software package, available online at http://www.srim.org

[23] L. Joulaud, J. Mangeney, J.-M. Lourtioz, P. Crozat and G. Patriarche , "Thermal stability of ion-irradiated InGaAs with (sub-) picosecond carrier lifetime", Appl. Phys. Lett., vol. 82, p. 856 , 2003.

[24] J. Mangeney, N. Stelmakh, F. Aniel, P. Boucaud and J.-M. Lourtioz, "Temperature dependence of the absorption saturation relaxation time in light- and heavy-ion-irradiated bulk GaAs", Appl. Phys. Lett., vol. 80, p. 4711, 2002.

[25] J. Mangeney, J. Lopez, N. Stelmakh, J.-M. Lourtioz, J.-L. Oudar and H. Bernas , "Subgap optical absorption and recombination center efficiency in bulk GaAs irradiated by light or heavy ions", Appl. Phys. Lett., vol. 76, p. 40, 2000.

[26] K. Nordlund, J. Peltola, J. Nord , J. Keinonen and R. S. Averback, "Defect clustering during ion irradiation of GaAs: Insight from molecular dynamics simulations", J. Appl. Phys., vol. 90, p. 1710, 2001.

[27] J. W. Tomm, V. Strelchuk, A. Gerhardt, U. Zeimer, M. Zorn, H. Kissel, M. Weyers and J. Jimenez, "Properties of As^+-implanted and annealed GaAs and InGaAs quantum wells: Structural and band-structure modifications", J. Appl. Phys., vol. 95, p. 1122, 2004.

[28] N. Stelmakh, J. Mangeney, A. Alexandrou, and E. L. Portnoi, "Intensity-invariant subpicosecond absorption saturation in heavy-ion irradiated bulk GaAs", Appl. Phys. Lett., vol. 73, p. 3715, 1998.

[29] J. Mangeney, L. Joulaud, P. Crozat, J.–M. Lourtioz and J. Decobert, “Ultrafast response (~2.2 ps) of ion-irradiated InGaAs photoconductive switch at 1.55 μm”, Appl. Phys. Lett. vol. 83, p. 5551, 2003.

[30] M. J. Lederer, V. kolev, B. L.-Davies, H. H. Tan and C. Jagadish , J.Phys D:Appl.Phys, vol. 34, p. 2455, 2001.

[31] O. Okhotnikov, A. Grudinin and M. Pessa, “Ultrafast-fibre laser systems based on SESAMs technology: new horizons and applications”, New J. Phys., vol. 6, p. 177, 2004.

[32] J. T. Gopinath, E. R. Thoen, E. M. Koontz, M. E. Grein, L. A. Kolodziejski, E. P. Ippen and J. P. Donnelly, “Recovery dynamics in proton-bombarded semiconductor saturable absorber mirrors”, Appl. Phys. Lett., vol. 78, p. 3409, 2001.

[33] M. Joschko, P. Langlois, E. R. Thoen, E. M. Koontz, E. P. Ippen and L. A. Kolodziejski, “Ultrafast hot-carrier dynamics in semiconductor saturable absorber mirrors”, Appl. Phys. Lett. , vol.76, p. 1383, 2000 .

[34] P. Langlois, M. Joschko, E. R. Thoen, E. M. Koontz, F. X. Kärtner, E. P. Ippen and L. A. Kolodziejski, “High fluence ultrafast dynamics of semiconductor saturable absorber mirrors”,Appl. Phys. Lett., vol. 75, p. 3841, 1999.

[35] B. E. A. Saleh and M. C. Teich, “Fundamentals of photonics”, John Willey & sons, Inc., New York, 1991.

[36] H. A. Haus, “ A theory of forced mode locking”, IEEE J. Quantum Electron., vol. 7, p. 323, 1975.

[37] H. A. Haus, “Short pulse generation in compact sources of ultrashort pulses”, Cambridge University Press, p. 1-56,1995,

[38] U. Keller, K. J. Weingarten, F. X. Kärtner, D. Kopf, B. Braun, I. D. Jung, R. Fluck, C. Hönninger, N. Matuschek and J. A. Aus, “Semiconductor saturable absorber mirrors (SESAMs) for femtosecond to nanosecond pulse generation in solid-state lasers”, IEEE J. selected Topics in Quantum Electronics, vol. 2, p. 435, 1996.

[39] J. Shah, T. C. Damen, B. Deveaud and D. Block, “Subpicosecond luminescence spectroscopy using sum frequency generation” Appl. Phys. Lett. , vol. 50, p.1307, 1987.

[40] L. V. Dao, M. Gal, G. Li, and C. Jagadish, “Dynamics of photoexcited holes in *n*-doped InGaAs/GaAs single quantum well”, Appl. Phys. Lett., vol. 71, pp-1849, 1997.

[41] N. V. Tkachenko, L. Rantala, A. Y. Tauber, J. Helaja, P. H. Hynninen and H. Lemmetyinen , ”Photoinduced electron transfer in phytochlorin-[60]fullerene dyads” J. Am. Chem. Soc., vol. 121, p. 9378, 1999.

[42] Y. -C. Chen, P. Wang, J. Coleman, D. P. Bour, K. K. Lee and R. G. Waters " carrier recombination rates in strained-layer InGaAs-GaAs quantum wells", IEEE Journal of Quantum Electronics, vol. 27, p. 1451, 1991.

[43] S. Marcinkevcius, U. Olin and G. Treideris , "Room temperature carrier recombination in InGaAs/GaAs quantum wells", J. Appl. Phys., vol. 74, p.3587, 1993.

[44] S. Marcinkevicius, J. siegert, R. Leon, B. Cechavicius, B. Magness and W. Taylor, "Changes in luminescence intensities and carrierdynamics induced by proton irradiation in $In_xGa_{1-x}As$/GaAs quantum dots", Phys. Rev. B., vol. 66, p. 235314, 2002.

[45] B. Deveaud, T. C. Damen , J. Shah and W. T. Tsang, "Capture of electrons and holes in quantum wells", Appl. Phys. Lett., vol. 52, p. 1886, 1988.

[46] D. Oberli, J. Shah, J. L. Lewell, T. C. Damen and N. Chand , "Dynamics of carrier capture in an InGaAs/GaAs quantum well trap", Appl. Phys. Lett. , vol. 54, p. 1028, 1989.

[47] B. Deveaud, D. Morris, A. R. X. Barros, P. Becker and J. M. Gerard, Opt. Quantum Electron, vol. 26, p. S679, 1994.

[48] R. Kersting, R. Schwedler, K. Wolter, K. Leo and H. Kurtz, "Dynamics of carrier transport and carrier capture in $In_{1-x}Ga_xAs$/InP heterostructures" Phys. Rev. B, vol. 46, p. 1639, 1992.

[49] X. Q. Zhou, K. Leo and H. Kurz, "Ultrafast relaxation of photoexcited holes in n-doped III-V compounds studied by femtosecond luminescence", Phys. Rev. B, vol. 45, p. 3886, 1992.

[50] K. Kalna and M. Mosko, "Electron capture in quantum wells via scattering by electrons, holes, and optical phonons", Phys. Rev. B., vol. 54, p. 17730, 1996.

[51] P. W. M. Blom, C. Smit, J. E. M. Haverkort, and J. H. Wolter, "Carrier capture into a semiconductor quantum well", Phys. Rev. B., vol.47, p. 2072, 1993.

[52] L. Davis, Y. L. Lam, Y. C. Chen, J. Singh and P. K. Bhattacharya, "Carrier capture and relaxation in narrow quantum wells", IEEE Journal of Quantum Electronics, vol. 30, p. 2560, 1994.

[53] C. Y. Sung, T. B. Norris, X. K. Zhang, Y. L. Lam, I. Vurgaftman, J. Singh and P. K. Bhattacharya,"Studies of carrier relaxation in low dimensional structures", Solid State Electronics, vol. 40, p. 751, 1996.

[54] M. H. Molony, J. Hegarty, L. Buydens, P. demeester, R. Grey and J. Woodhead, " Carrier lifetimes in strained InGaAs/(Al)GaAs multiple quantum wells", Appl. Phys. Lett. , vol. 62, p. 3327, 1993.

[55] B. Elman, Emil S. Koteles, P. Mekman, C. Jagannath, C. A. Armiento, and M. Rothman, "

Effect of heat tratment on InGaAs/GaAs quantum wells", J. Appl. Phys., vol. 68, p. 1351, 1990.

[56] G. Bacher, C. Hartmann, H. Schweizer, T. Held, G. Mahler and H. Nickel, "Exciton dynamics in $In_xGa_{1-x}As/GaAs$ quantum-well heterostructures: Competition between capture and thermal emission", Phys. Rev. B., vol. 47, p. 9545, 1993.

[57] L. V. Dao, M. Gai, H. Tan and C. Jagadish, " Carrier capture into InGaAs/GaAs quantum wells via impurity mediated resonant tunneling", Appl. Phys. Lett., vol. 72, p. 2008, 1998.

[58] S. Jin and A. Li, "Recombination kinetics of excess carriers in semiconductor quantum wells", J. Appl. Phys., vol. 81, p. 7357, 1997.

[59] B. K. Ridley, " Kinetics of radiative recombination in quantum wells", Phys. Rev. B.,vol 41, p. 12190, 1990.

[60] J. Wang, U. A. Griesibger and H. Schweizer, "Direct determination of carrier capture times in low-dimensional semiconductor lasers: The role of quantum capture in high speed modulation", Appl. Phys. Lett., vol. 69, p. 1585,1996.

[61] A. Morin. B. Deveaud, F. Clerot, K. Fujiwara and K. Mitsunaga," Capture of photoexcited carriers in a single quantum well with different confinement structures", IEEE Journal of Quantum Electronics, vol. 27, p. 1669, 1991.

[62] Y. Ohzumi, T. Tsuruoka, and S. Ushioda, "Formation of misfit dislocations in GaAs/InGaAs multiquantum wells observed by photoluminescence microscopy", J. Appl. Phys., vol. 92, p. 2385, 2002.

[63] S. Jin, Y. Zheng, and A. Li, "Characterization of photoluminescence intensity and efficiency of free excitons in semiconductor quantum well structures" J. Appl. Phys., vol. 82, p. 3870, 1997.

[64] R. S. Averback and T. Diaz de la Rubia, "Displacement damage in irradiated metals and semiconductors in Solid State Physics", edited by H. Ehrenfest and F. Spaepen, vol 51, p. 281-402, Academic Press, New York, 1998.

[65] D. Kanjilal, "Swift heavy ion-induced modification and track formation in materials" current science, vol. 80, p. 1560, 2001.

Appendix 1.

Publication 1.

V. D. S. Dhaka, N. V. Tkachenko, E. -M. Pavelescu, H. Lemmetyinen, T. Hakkarainen, M. Guina, J. Konttinen, O. Okhotnikov, M. Pessa, K. Arstila and J. Keinonen, "*Ni+-irradiated InGaAs/GaAs quantum-wells: picosecond carrier dynamics*", **New J. Phys.**, vol. 7, 131, 2005.

Appendix 2.

Publication 2.

V. D. S. Dhaka, N.V. Tkachenko, H. Lemmetyinen, E. -M. Pavelescu, J. Konttinen, M. Pessa, K. Arstila and J. Keinonen, "*Room-temperature self-annealing of heavy-ion-irradiated InGaAs/GaAs quantum wells* ", **IEE Electron. Lett.**, vol. 41, pp. 1304-1305, 2005.

Appendix 3.

Publication 3.

T. Hakkarainen, E. -M. Pavelescu, K. Arstila, **V. D. S. Dhaka**, T. Hakulinen, R. Herda, J. Konttinen, N. Tkachenko, H. Lemmetyinen, J. Keinonen and M. Pessa, *"Optical properties of ion irradiated and annealed InGaAs/GaAs quantum wells and semiconductor saturable absorber mirrors"*, **J. Phys. D: Appl. Phys.**, vol. 38, pp. 985-989, 2005.

Appendix 4.

Publication 4.

E. -M. Pavelescu, T. Hakkarainen**, V. D. S. Dhaka**, N. V. Tkachenko H. Lemmetyinen, T. Jouhti and M. Pessa**,** *"Influence of As pressure on photoluminescence and structural properties of GaInNAs/GaAs quantum wells grown by molecular beam epitaxy"*, **J. Crystal Growth**, vol. 281, pp. 249-254, 2005.

Appendix 5.

Publication 5.

V. D. S Dhaka, N. V. Tkachenko, H. Lemmetyinen, E. -M. Pavelescu, S. Suomalainen, M Pessa, K. Arstila, K. Nordlund and J. Keinonen, "*Ultrafast dynamics of Ni^+-irradiated and annealed GaInAs/InP multiple quantum wells"*, **J. Phys. D: Appl. Phys.**, vol. 39, pp. 2659-263, 2006.

Appendix 6.

Publication 6.

V. D. S. Dhaka, N. V. Tkachenko, H. Lemmetyinen, E. -M. Pavelescu, M. Guina, A. Tukiainen J. Konttinen, M. Pessa, K. Arstila, J. Keinonen and K. Nordlund, "*Effects of heavy-ion and light-ion irradiation on the room-temperature carrier dynamics of InGaAs/GaAs quantum wells"*, **Semiconductor Science and Technology**, vol. 21, pp. 661-664, 2006.

Appendix 7.

Publication 7.

V. D. S. Dhaka, N. V. Tkachenko, E. -M. Pavelescu, H Lemmetyinen, M. Pessa, "*Effect of growth temperature and post-annealing on carrier dynamics in GaIn(N)As/GaAs quantum wells"*, **Solid State Electronics** (Submitted)

Tampereen teknillinen yliopisto
PL 527
33101 Tampere

Tampere University of Technology
P.O. Box 527
FIN-33101 Tampere, Finland